*minerals*

MDPI

*Article*

# Thermochronology of the Kalba–Narym Batholith and the Irtysh Shear Zone (Altai Accretion–Collision System): Geodynamic Implications

**Alexey Travin [1,2,*], Mikhail Buslov [1], Nikolay Murzintsev [1], Valeriy Korobkin [3], Pavel Kotler [1], Sergey V. Khromykh [1] and Viktor D. Zindobriy [1]**

[1] V.S. Sobolev Institute of Geology and Mineralogy SB RAS, Novosibirsk 630090, Russia; buslov@igm.nsc.ru (M.B.); murzintsevng@gmail.com (N.M.); pkotler@yandex.ru (P.K.); serkhrom@igm.nsc.ru (S.V.K.); dobriyvd@igm.nsc.ru (V.D.Z.)
[2] Faculty of Physics and Technology, Department of Geophysical Systems, Novosibirsk State Technical University, Novosibirsk 630073, Russia
[3] School of Geology, Kazakh-British Technical University, Almaty 050000, Kazakhstan; korobkin_vv@mail.ru
* Correspondence: travin@igm.nsc.ru; Tel.: +7-913-0099973

**Abstract:** The granitoids of the Kalba–Narym batholith and the Irtysh shear zone (ISZ) are among the main geological features of the late Paleozoic Altai accretion–collision system (AACS) in Eastern Kazakhstan. Traditionally, it is believed that late Paleozoic strike-slip faults played a pivotal role at all stages of the development of the AACS, they were supposed to control deformation, magmatism, and ore deposits. This work is devoted to solving the problem of the tectonic evolution of the AACS based on the reconstruction of the thermal history of granitoids of the Kalba–Narym batholith in connection with the Chechek metamorphic dome structure, which is one of the highly metamorphosed blocks mapped within the ISZ. The new geological and geochronological data presented in this work allowed us to establish the sequence of formation of the Kalba–Narym granitoid batholith and link it with the evolution of the Irtysh shear zone (ISZ). It was revealed that in the late Carboniferous–early Permian (312–289 Ma), during the NE–SW compression, the Irtysh shear zone formed as a gently dipping thrust system into which gabbro of the Surov massif intruded. The combined manifestation of magmatic and tectonic processes caused the formation of tectonic mélange with cataclastic gabbro and metamorphic rocks of the Chechek metamorphic dome structure (312–289 Ma). Compression caused the formation of a cover-thrust structure. The thickening of the crust under the probable thermal action of the Tarim plume led to the formation of the early Permian Kalba–Narym batholith (297–284 Ma) within the Kalba–Narym terrane. Denudation of the orogen occurred before the Early Triassic (280–229 Ma). In this way the sequence of formation of the Kalba–Narym batholith and the ISZ is consistent with the concepts of the stages of plume-lithosphere interaction within the AACS under the influence of the late Carboniferous–early Permian Tarim igneous province, but in the cover-thrust tectonic setting.

**Keywords:** Eastern Kazakhstan; Altai accretion–collision system; thermochronology; $^{40}Ar/^{39}Ar$ dating; Kalba–Narym batholith; Irtysh shear zone; cover-thrust tectonics

check for updates

Academic Editor: Paris Xypolias

Received: 20 November 2024
Revised: 24 February 2025
Accepted: 25 February 2025
Published: 26 February 2025

**Citation:** Travin, A.; Buslov, M.; Murzintsev, N.; Korobkin, V.; Kotler, P.; Khromykh, S.V.; Zindobriy, V.D. Thermochronology of the Kalba–Narym Batholith and the Irtysh Shear Zone (Altai Accretion–Collision System): Geodynamic Implications. *Minerals* **2025**, *15*, 243. https://doi.org/10.3390/min15030243

**Copyright:** © 2025 by the authors. Licensee MDPI, Basel, Switzerland. This article is an open access article distributed under the terms and conditions of the Creative Commons Attribution (CC BY) license (https://creativecommons.org/licenses/by/4.0/).

## 1. Introduction

The late Paleozoic Altai accretion–collision system (AACS) is traditionally distinguished on the territory of Eastern Kazakhstan [1–5], which is part of the large Central Asian fold belt (CAFB). CAFB resulted from the accretion–collision interactions of the

Paleo-Asian Ocean (PAO) plate with the Siberian and Kazakh paleocontinents. The belt contains fold zones of different ages, formed during the Vendian–Paleozoic by successive accretion and collision of island arcs, microcontinents, and oceanic plateaus to the Siberian continent [1,6–14]. According to [15–22], a single Vendian–Paleozoic subduction zone developed in the PAO over which the Kipchak arc formed. During the Paleozoic, due to the drift and rotation of the Siberian and East European continents, deformations of the arc occurred, manifested in the formation of oroclinal bends and a large-amplitude strike-slip system. The most important episodes of strike-slip movements of the terranes are the late Carboniferous and then late Permian. According to this model, fragments of the Kipchak arc, originally framing the Siberian and East European continents, were combined in the CAFB (Altaids, according to [15]) since the late Paleozoic.

The late Precambrian–Paleozoic collisional and accretionary orogenies have been distinguished in the geodynamic zoning of the CAFB (Figure 1) [23–25].

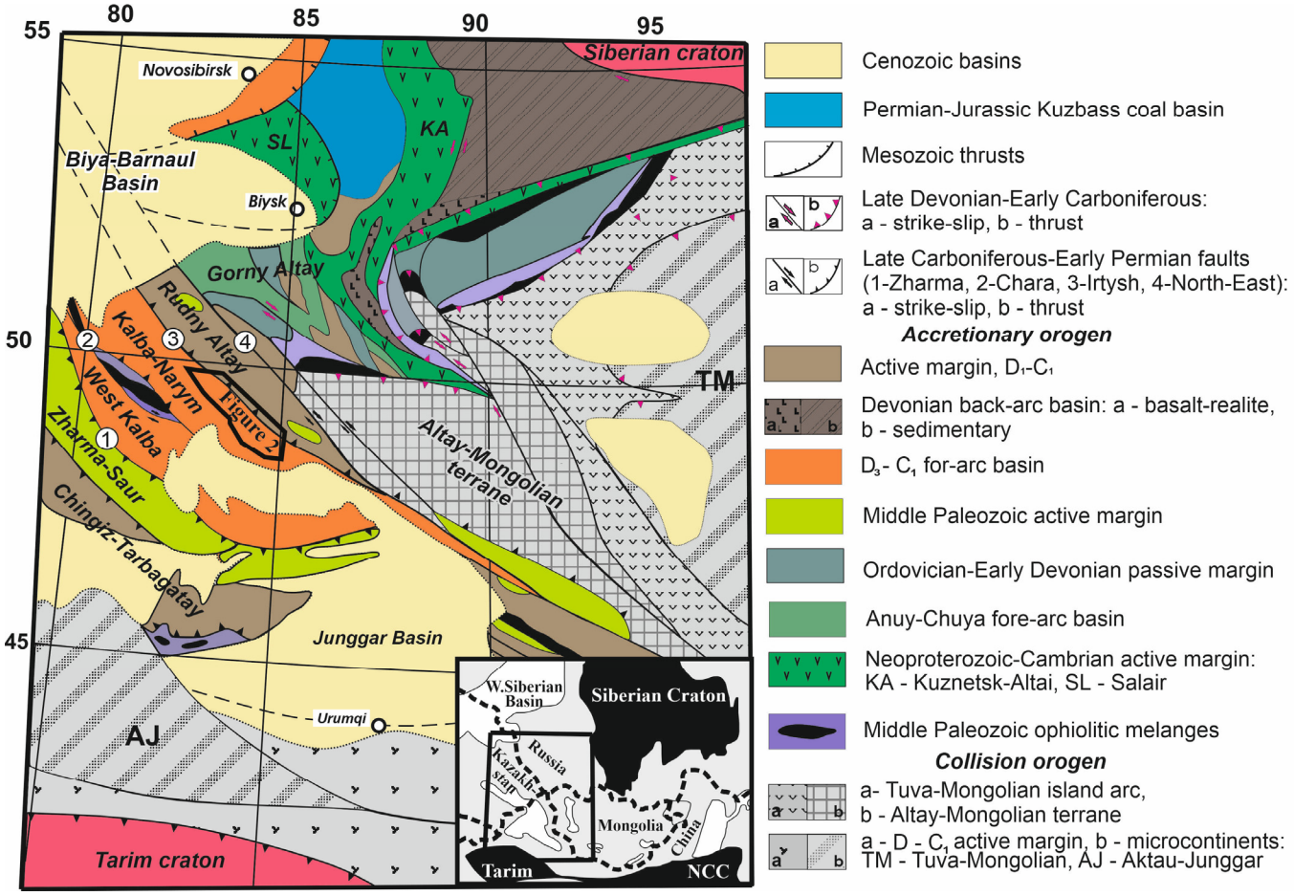


**Figure 1.** Geodynamic scheme of the Central Asian folded belt and the position of the studied object (Figure 2) (after [24,25]).

A characteristic feature of collisional orogens of the CAFB is the presence of Precambrian microcontinents of the Gondwana group among the units involved in the collision. At the same time, a characteristic feature of accretion orogens of the CAFB is the absence of microcontinents of the Gondwana group among the units involved in the collision [23–25]. If the two types of orogens mentioned above have been relatively preserved near the Siberian craton (Altai-Sayan region, Tuva, Mongolia, Transbaikalia), then in the rest of the CAFB their position and relationship are largely disrupted by late Paleozoic thrusting and

strike-slip faulting. To the greatest extent, the primary structure is distorted by late fault tectonics within the AACS (Figure 1).

Several large fault and/or shear zones (depending on the depth of the erosion section) of the northwestern strike are manifested in the AACS. The largest among them are Zharma, Chara, Irtysh, Northeastern, and others. They limit large (with a width of many tens to hundreds of km) terranes, such as Chingiz–Tarbagatai, Zharma–Saur, Zapadno–Kalbin, Kalba–Narym, Rudny–Altai, and Gorny–Altai (Figure 1). These fault zones controlled tectonic deformations, metamorphism, magmatism, and ore deposits in the AACS [1,2,4,13,14,26–39]. According to [13], in the AACS in the late Paleozoic–early Mesozoic, accretion–collision processes manifested themselves as structure-forming factors, while the Tarim and Siberian plumes played the role of energy sources [40–51].

If the large late Paleozoic strike-slip systems of the northern part of the Central Asian Basin are well studied and characterized [4,24,27,28,52,53], then the accompanying and (or) preceding covering structures have still been poorly identified [24,52,54]. In the case of a high degree of denudation, vertical root zones of cover and shear structures are preserved on the erosion section affecting the crystalline basement. This makes it difficult to decipher the initial structure of the region, especially if faults of different kinematics and ages are superimposed on each other. In this case, in addition to detailed structural and material studies of fault zones, thermochronological analysis, especially of igneous and metamorphic rocks, which are usually formed in the roots of these orogenies, becomes important.

Thermochronological analysis is based on the use of a set of dating methods for minerals characterized by different closing temperatures [55]. A comparison of the recorded age values of isotopic systems with their closure temperatures, taking into account the range of variations in the temperature gradient of the continental crust (30–12°/km [56]), allows us to obtain an idea of the position of the rock in depth at various time intervals.

A comparison of U/Pb dating of zircon, $^{40}Ar/^{39}Ar$ dating of minerals with different closing temperatures of the K/Ar isotope system (amphibole, mica, feldspar), and Apatite Fission Track (AFT) dating enables an estimate of the thermal history of rocks [57,58], which differs in the case of manifestations of thrust and strike-slip structures. The cover structures caused by thrust processes are characterized by a large vertical component coherent with the shortening and, as a result, a higher cooling rate on the thermal curve reconstructed based on the closure of the sequence of isotope systems and minerals. For strike-slip structures, the predominant component of movement is horizontal, so it is logical to expect that the vertical component of rock movement will not be as high as in the case of thrust structures. In other words, the rock systems of the cover and strike-slip type should be characterized by different denudation rates. Based on this, it can be confidently stated that the thermal history of rocks, for example, granitoid batholiths, containing the largest number of minerals of various closing temperatures of isotope systems, supplemented, if possible, by thermobarometric reconstructions, can serve as an independent source of information about the tectonic evolution of fold regions.

This article is devoted to the reconstruction of the thermal history of the late Paleozoic Kalba–Narym batholith in relation to the manifestation of the Surov gabbroid massif and the Chechek metamorphic complex (granite–gneiss structure), as well as the evolution of the fault tectonics of the ISZ. In order to understand which stages of the ISZ evolution are associated with the formation and further exhumation of the Kalba–Narym batholith, the results of U/Pb isotope dating of zircon, $^{40}Ar/^{39}Ar$ dating of amphibole, biotite, and feldspar, and AFT dating of the listed geological formations are used. According to the authors of the article, the results obtained can make a significant contribution to solving

the problem of the tectonic evolution of the AACS and, accordingly, are taken into account in global geodynamic models of the tectonic evolution of the CAFB as a whole.

## 2. Geological Framework

### *2.1. The AACS Formation*

AACS formed between Siberian and Kazakh paleocontinents [1,2,5,9,10,13] with the closure in the early Carboniferous of the Ob-Zaisan Paleo-Oceanic basin. The final formation of the fold structure occurred at the end of the early Carboniferous (Serpukhov), which is recorded by the appearance of continental molasses deposits of the Bashkir stage with basal conglomerates in localized intermountain depressions. The late Paleozoic active margin of the Siberian continent corresponds to the Rudny–Altai island-arc system, characterized by late Silurian–early Carboniferous volcanogenic sedimentary and granitoid complexes. From the northeast, it is separated by the North-East Fault from the Caledonian Gorny–Altai terrane, and from the southwest, through the ISZ, it is adjacent to the pre-arc turbidite of the Kalba–Narym terrane (Figures 1 and 2). The source of the material for the Kystav–Kurchum ($D_2$gv) and Takyr ($D_3$-$C_1$) formations suites was probably the Rudno–Altaisk island arc system [3,9].

The processes of soft collision interaction of the Siberian and Kazakh continents (not reaching the direct collision of hard continental blocks) caused the deformation of volcanogenic sedimentary rocks of the AACS and their compression, close to the isoclinal folds of the northwestern strike of the axial planes, inclined generally to the northeast [2,10]. In the early Permian, granitoids of the Kalba batholith were formed within the Kalba–Narym terrane and in its marginal part—the ISZ, including the Surov gabbro massif and the Chechek metamorphic complex (Figure 2). The collision of the Kazakh and Siberian plates took place when they rotated clockwise relative to each other, which led to an important structural role of large-amplitude shear displacements at all stages of the AACS development [4,12,13,15,17,18,37,38,46,47,59–62]. They formed the Zharma, Chara, Irtysh, and Northeastern shear zones (Figure 1). The strike-slip structures were accompanied by less amplitude thrust movements along the feathering faults of the sub-latitudinal orientation.

The largest trans-regional tectonic strike-slip displacement in Central Asia is considered to be the Irtysh Shear Zone (ISZ) [4,12,13,17,18,31–36]. Based on structural-petrological and geochronological ($^{40}Ar/^{39}Ar$) studies, two episodes of large-amplitude left-lateral plastic and brittle-plastic deformations with ages of 285–275 and 270–260 Ma have been identified [38]. For the Kalba batholith belt located on the southwestern flank of the ISZ, estimates of the age of formation based on U/Pb dating by zircon fall within the range of 290–274 Ma [38,39]. On this basis, as well as based on structural observations, the sin-tectonic nature of the Kalba batholith belt is assumed [13]. At the same time, the synchronicity of the formation of batholith granitoids with the formation of the Tarim large igneous province [40–45] and the close geographical location suggested that the Tarim mantle plume is the most likely energy source that caused the formation of the Kalba–Narym batholith [46,47]. Thus, an interconnected reconstruction of the history of the formation and further tectonic evolution of the ISZ and the Kalba–Narym batholith is relevant.

Throughout the ISZ, deeply metamorphosed tectonic blocks were mapped, for example, Predgornensky, Chechek, and Kurchum (Figure 2a). There are different ideas about the age and genesis of these blocks. Some authors believe that they are exhumed fragments of the Precambrian basement [48,49]. According to another concept, the blocks were formed because of the thermal action of the gabbro of the Irtysh complex, which intruded into the ISZ [50,51]. Within the Chechek structure, the gabbro of the Irtysh complex manifested itself as a large Surov massif (Figure 2).

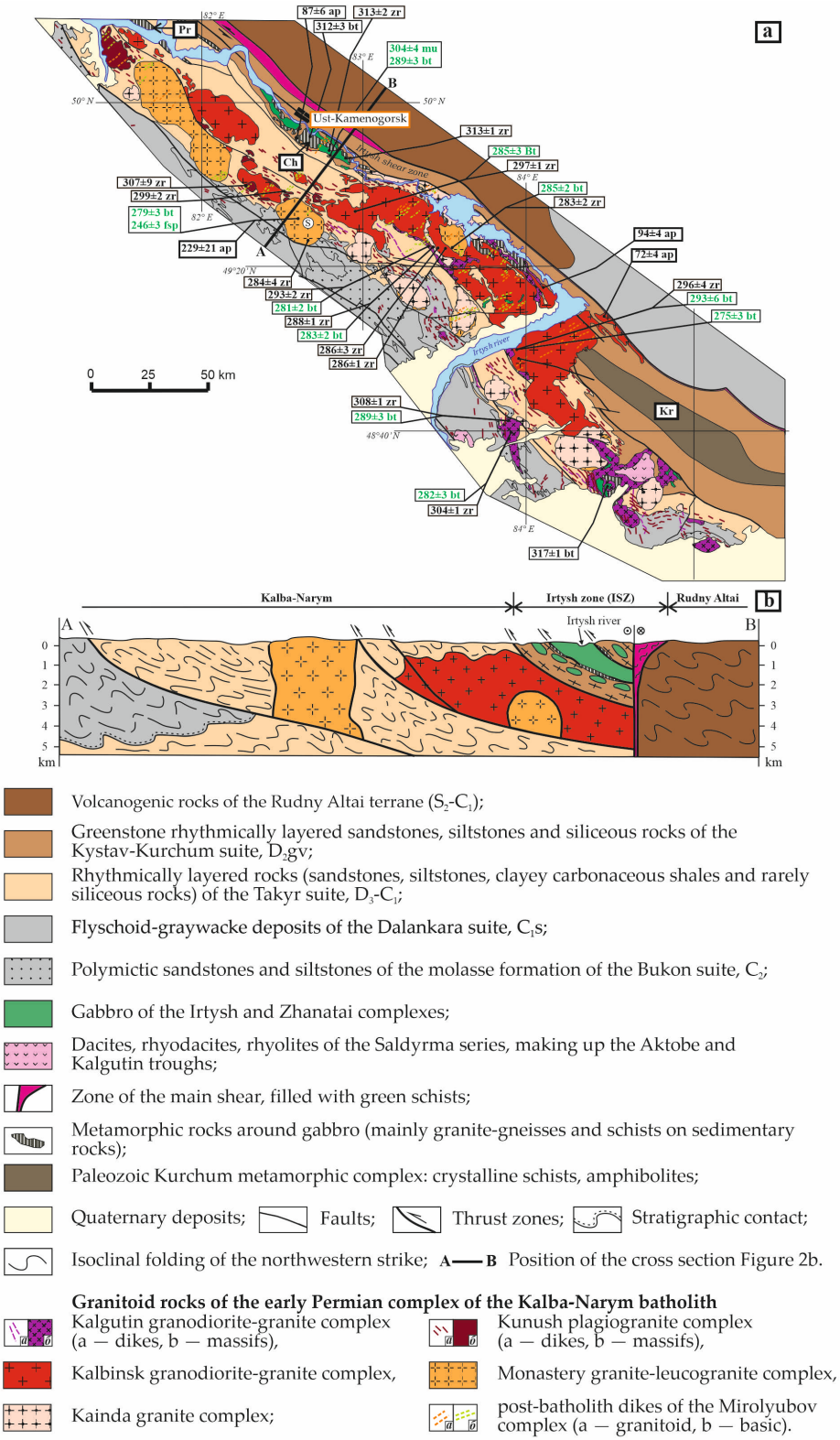


**Figure 2.** (**a**) Scheme of the geological structure of the Irtysh shear zone and the Kalba–Narym batholith according to [39], modified. Bold rectangles with arrows show blocks of deeply metamorphosed rocks within the ISZ: Pr—Predgornensky, Ch—Chechek, and Kr—Kurchum. The numbers in the rectangles are geochronological data (million years old). The dates for zircon (zr) were obtained by U/Pb, for feldspar (fsp), muscovite (mu), and biotite (bt) were obtained by the $^{40}Ar/^{39}Ar$ method, and for apatite by the FT method. The dates obtained in this work are highlighted in green. The letter S in the circle indicates the Sebinsky massif of the Kalba–Narym batholith. (**b**) Schematic section of the Kalba–Narym terrane, the Irtysh shear zone, and the outskirts of the Rudny Altai terrane.

Although the main stages of the geodynamic evolution of the Kalba–Narym batholith, Rudny–Altai terrane, and the ISZ considered in this article have been generally identified, many unresolved questions remain, for example, about the role of the ISZ in the formation of the Kalba–Narym granitoid batholith, as well as about the role of the ISZ in its subsequent post-magmatic history. There are still different interpretations for the evolution of the kinematics of deformations of the ISZ. In a number of works, the point of view is expressed that the ISZ is an important structure in the framework of the Central Asian Orogenic Belt (CAOB). It represents the site of the final collision of Kazakhstan with Siberia during Hercynian times and records up to 1000 km of lateral displacement during subsequent reorganization in the CAOB edifice [4,12,13,17,18,31].

The authors of the following works believe that the history of ISZ includes three episodes of late Paleozoic deformation representing orogenic thickening, collapse, and transpressional deformation. On a larger scale, late Paleozoic shearing accommodated the eastward migration of internal segments of the western CAOB, possibly associated with the amalgamation of multiple arc systems and continental blocks [22,25,33,35,36]. The systematic reconstruction of the cooling history of the granitoid massifs of the Kalba–Narym batholith is still lacking, as well as a model for its denudation.

### *2.2. The Kalba–Narym Batholith*

The granitoids of the Kalba–Narym zone, forming one of the largest batholiths in the western Central Asian fold belt, occupy a significant part of the area of the Kalba–Narym terrane (>40,000 km$^2$). According to geophysical data, the thickness of granitoid massifs ranges from 2 to 12 km with a predominance of 7–10 km [63,64].

The granitoid Kalba–Narym batholith includes the Kalgutin granodiorite–granite complex, and the Kunush–plagiogranite complex, the Kalba granodiorite–granite complex, the Monastery granite–leucogranite complex. The batholith is intruded by "post-batholith" dikes of the Mirolyubov complex. Also within the Kalba–Narym terrane near Ust-Kamenogorsk are gabbro of the Surov massif of the Irtysh complex and metamorphic rocks of the Chechek granite–gneiss structure, distinguished as part of the ISZ (Figure 2) [46,60,61,65–67].

### *2.3. The Irtysh Gabbro Complex*

In the marginal part of the Kalba–Narym terrane, within the ISZ, outcrops of gabbro of the Surov massif (313 ± 1 Ma) [61]) close in age with the Chechek complex are found (312 ± 3 Ma) [12,65,66]. The origin of metamorphic rocks is directly related to the episode of the introduction and formation of the Surov gabbro lopolith, which provided the necessary heating and melting of the overlying strata, and after consolidation (312 ± 3 Ma ago)—reservation and "protection" from late (~280 and ~260 Ma) large-scale shear deformations along the ISZ [65,66].

Rocks of the early Carboniferous Irtysh gabbro complex, of which the Surov massif is a part [61,68,69], intrude middle Devonian sedimentary rocks (Kystav–Kurchum and Takyr suites). Their contacts are intrusive in the case of large gabbro bodies and predominantly tectonic in the case of small bodies. The small bodies of gabbro are most often rootless tectonic sheets or boudin-like bodies among metamorphic rocks. The Surov intrusion is lopolite shaped (Figures 2 and 3) and has mainly NE dipping magmatic layering. Its basal series exposed in the southern part of the intrusion consists of pre dominant melanocratic gabbro and minor amounts of ultramafic rocks (mainly olivine cumulate).

### *2.4. The Chechek Metamorphic Complex*

Near Ust'-Kamenogorsk, the Surov gabbro is adjacent to the gneiss and diatectite of the Chechek metamorphic complex of epidote–amphibolite to amphibolite facies [65]. The core of this complex consists mainly of granite gneiss and numerous synmetamorphic granite veins. The presence of garnet, sillimanite, and cordierite in granite gneiss, as well as granoblastic and coronite textures, records a prolonged heating effect. Minerals in the center of the Chechek complex formed at T = 665–720 °C and P = 0.4–0.6 GPa, in the upper amphibolite facies conditions. Thus, the metamorphism was a contact one and was a consequence of the thermal effect of gabbro [65].

## 3. Materials and Methods

Geological field research was conducted mostly through hiking trails, documenting rock relationships, sketching key outcrops, and sampling. The testing was carried out on the bedrock outcrops or on the blocky ruins of the same rocks directly on the bedrock outcrops. The freshness of the selected samples was visually controlled by the gloss of micas, amphiboles, etc. Hand-held GPS receivers were used for coordinate control of the sampling points. Samples were taken from various parts of the cover-thrust structure of the region. The most important of them are the granitoid complexes of the Kalba–Narym terrane, the Surov gabbro massif, and the Chechek metamorphic complex. Whenever possible, rock samples were taken that contain the maximum amount of various minerals (zircon, apatite, amphibole, mica, feldspars), differing in the closing temperatures of isotopic systems. The obtained results of the dating of these minerals eventually made it possible to create a tectonothermal reconstruction of the cover-thrust structure.

In order to reconstruct the history of the formation of the cover-thrust structure of the Kalba–Narym terrane and, in general, the AACS, we compared thermochronological data for granitoid complexes of the Kalba–Narym batholith, as well as for the Surov Gabbro massif and the Chechek metamorphic complex. Eleven samples of granitoid complexes of the Kalba–Narym batholith were used, which were previously characterized in detail using petrological and geochemical data, and for which the age of zircon was determined by the U/Pb method [38]. Monofractions of biotite and muscovite were selected from a sample of cataclased gabbro (sample B-23-146).

The thermochronological approach is based on the kinetic parameters of daughter isotopes measured in laboratory conditions and assumes the immutability of the crystal structure of the mineral while considering the case when the closure temperature is significantly lower than the temperature of the formation of the mineral—$T_c < T_f$. In this case, the obtained dating corresponds to the closure time of the corresponding isotope system. In some situations, the ratio between the closure temperature of the isotope system $T_c$ and the formation temperature $T_f$ of the dated mineral phase is the opposite—$T_c > T_f$. For example, the U/Pb dates for zircon correspond to this case. With this ratio, the obtained dating directly corresponds to the age of formation of the dated mineral phase, namely, zircon.

$^{40}Ar/^{39}Ar$ biotite dating was performed on 11 samples (B-23-146, K-14-16, X-1041, X-1042, X-1044, X-1045, X-1047, X-1052, X-1056, 2463, 2458), whereas feldspar was used only once (sample K-14-19). Sample B-23-146 was instead dated with both biotite and muscovite. Petrological and petrochemical descriptions of the samples are given in the relevant publications (see Table 1). Minerals for $^{40}Ar/^{39}Ar$ dating were extracted by the conventional techniques of magnetic and density separation at the V.S. Sobolev Institute of Geology and Mineralogy (Novosibirsk, Russia).

**Table 1.** Summary of thermochronological data for granitoids of the Kalba–Narym batholith and the Chechek granite–gneiss structure.

| Sample/ Massif | Complex/ Rock/Mineral * | Method ** | Age (Ma) | Closure/ Formation T (°C) *** | Reference |
|---|---|---|---|---|---|
| X-1052 | Kalgutin/ granodiorite/zrn | $U/Pb_L$ | 308 ± 2 | ~$850_f$ | [38] |
| X-1052 Kurchum | Kalgutin/ granodiorite/bt | $^{40}Ar/^{39}Ar$ | 289 ± 3 | $330_c$ | This work |
| X-1047 | Kalgutin/ granodiorite/zrn | $U/Pb_L$ | 303 ± 1 | ~$850_f$ | [38] |
| X-1047 Kurchum | Kalgutin/ granodiorite/bt | $^{40}Ar/^{39}Ar$ | 282 ± 3 | $330_c$ | This work |
| X-1056 | Kalba/granite/zrn | $U/Pb_L$ | 297 ± 1 | ~$806_f$ | [38] |
| X-1056/ Asubulak | Kalba/granite/bt | $^{40}Ar/^{39}Ar$ | 285 ± 2 | $330_c$ | This work |
| X-1045 | Kalba/granodiorite/zrn | $U/Pb_L$ | 297 ± 1 | ~$806_f$ | [38] |
| X-1045 Chernovin | | $^{40}Ar/^{39}Ar$ | 281 ± 2 | $330_c$ | This work |
| X-1042 | Kalba/granite/zrn | $U/Pb_L$ | 286 ± 3 | ~$806_f$ | [38] |
| X-1042 Chernovin | Kalba/granite/bt | $^{40}Ar/^{39}Ar$ | 268 ± 2 | $330_c$ | This work |
| Narym | Kalba/granite/zrn | $U/Pb_L$ | 296 ± 4 | ~$806_f$ | [5] |
| 2458 | Kalba/granite/bt | $^{40}Ar/^{39}Ar$ | 275 ± 3 | $330_c$ | This work |
| 2463 | Kalba/granite/bt | $^{40}Ar/^{39}Ar$ | 283 ± 3 | $330_c$ | This work |
| X-1044 | Kalba/granite/zrn | $U/Pb_L$ | 288 ± 1 | ~$806_f$ | [38] |
| X-1044 Chernovin | Kalba/granite/bt | $^{40}Ar/^{39}Ar$ | 282 ± 2 | $330_c$ | This work |
| X-1041 | Monastery/ leucogranite/zrn | $U/Pb_L$ | 283 ± 2 | ~$810_f$ | [38] |
| X-1041 Voylochev | Monastery/ leucogranite/bt | $^{40}Ar/^{39}Ar$ | 285 ± 2 | $330_c$ | This work |
| 8-03-10 Sebin | Monastery/ leucogranite/zrn | $U/Pb_L$ | 284 ± 4 | ~$810_f$ | [38] |
| KA-14-18 | Monastery/ leucogranite/bt | $^{40}Ar/^{39}Ar$ | 280 ± 2 | $330_c$ | This work |
| KA-14-18 Sebin | Monastery/ leucogranite/fsp | $^{40}Ar/^{39}Ar$ | 243 ± 3 | $250_c$ | This work |
| KA-21-345 KA-21-346 KA-21-347 Sebin | Monastery/ leucogranite/ap | FST | Average 229 ± 21 | $110_c$ | [70] |
| X-1414 Surov intrusion | Irtysh/gabbronorite/zrn | $U/Pb_L$ | 313 ± 1 | >$900_f$ | [61] |
| X-1207 Surov intrusion | Irtysh/gabbrodiorite/zrn | $U/Pb_L$ | 313 ± 1 | >$900_f$ | [61] |

**Table 1.** *Cont.*

| Sample/ Massif | Complex/ Rock/Mineral * | Method ** | Age (Ma) | Closure/ Formation T (°C) *** | Reference |
|---|---|---|---|---|---|
| E-32 Chechek | Chechek/granite-gneiss/ms | $^{40}Ar/^{39}Ar$ | 312 ± 3 | $360_c$ | [65] |
| KZ-06 Chechek | Chechek/granite-gneiss/ap | FST | 87 ± 6 | $110_c$ | [17] |
| B-23-146 | Chechek/gabbro tectonite/ms | $^{40}Ar/^{39}Ar$ | 304 ± 4 | $360_c$ | This work |
| B-23-146 Surov intrusion | Chechek/gabbro tectonite/bt | $^{40}Ar/^{39}Ar$ | 289 ± 3 | $330_c$ | This work |

* The following designations are used in the table: zrn—zircon, ms—muscovite, bt—biotite, fsp—feldspar, ap—apatite. ** U/Pb zircon dating was performed using the ICP laser ablation mass spectrometry method ($U/Pb_L$). *** $T_c$ is the closing temperature of the corresponding isotope system; $T_f$ is the temperature of formation of the corresponding mineral phase.

$^{40}Ar/^{39}Ar$ dating of monomineral fractions was carried out at the Analytical Center for Multi-element and Isotope Studies (Novosibirsk, Russia) as in [57]. Samples were wrapped in aluminum foil together with biotite MCA-11 standard monitor samples, placed in quartz capsules, vacuumed, and sealed. For muscovite MCA-11, as a result of its calibration using muscovite Bern 4m and biotite LP-6, we assumed an average age value of 311.0 ± 1.5 Ma. The error of the calculated value of J, characterizing the neutron flux value for each of the positions within the ampoule, did not exceed 0.5%. The capsules were irradiated by fast neutrons in a Cd-lined tube of the IRT-T nuclear reactor at Tomsk Polytechnical University, in Tomsk, Russia. The samples were subjected to stepwise heating in a quartz tube using an external tubular resistance furnace. A chromel-alumel thermocouple was used to control the temperature with the accuracy of ±3 °C. The $^{40}Ar$ and $^{36}Ar$ blank runs (10 min at 1200 °C) did not exceed $3 \times 10^{-10}$ and $0.003 \times 10^{-10}$ $ncm^3$, respectively. Argon cleaning was performed using ZrAl-SAES getters (SAES Advanced Technologies Spa, Avezzano, Italy). The argon isotope composition was measured on a Micromass Noble Gas 5400 mass spectrometer (Micromass UK Limited, Wilmslow, UK), to an accuracy of ±1σ. The contribution of interfering Ar isotopes formed together with $^{39}Ca$ and $^{40}K$ was estimated using the coefficients of $(^{39}Ar/^{37}Ar)_{Ca} = 0.001279 \pm 0.000061$, $(^{36}Ar/^{37}Ar)_{Ca} = 0.000613 \pm 0.000084$, and $(^{40}Ar/^{39}Ar)_K = 0.0191 \pm 0.0018$. The plateau ages were calculated in Isoplot-3 [71], as weighted average values over at least three successive temperature steps. The results were interpreted with reference to the conventional criteria [72]. Analytical error is specified at the level of 1σ.

## 4. Results

### *4.1. The Fieldwork*

The fieldwork of our research over the past few years revealed that in the area of Ust-Kamenogorsk, the boundary of the Irtysh gabbro complex and the metamorphic rocks of the Chechek complex is represented by a thrust (Figure 3). The plunging of the thrust planes is defined as north-eastern. They are transformed into dome-shaped folds. The thrust structure is everywhere disrupted by right-lateral shifts of north-eastern strike, deforming it into Z-shaped folds with amplitudes of up to a few tens of cm. The shear deformations are most fully manifested at the boundary with the Rudny–Altai terrane, where they are represented by a zone of green schists with a thickness of up to many hundreds of meters.

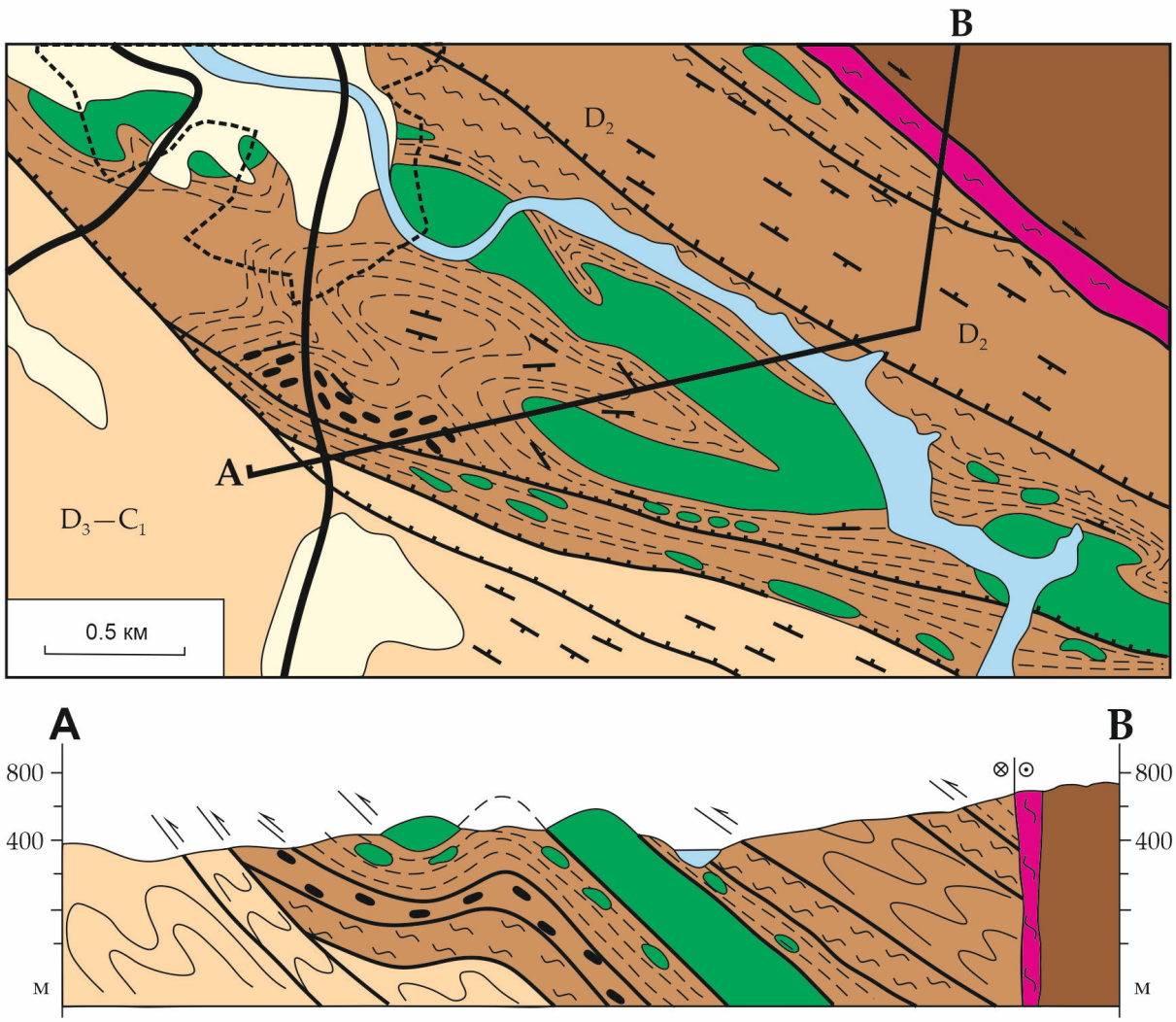


volcanogenic rocks of the Rudny Altai terrane ($S_2$-$C_1$)

Greenstone rhythmically layered sandstones, siltstones and siliceous rocks of the Kystav-Kurchum suite, $D_2$gv

Rhythmically layered rocks (sandstones, siltstones, clayey carbonaceous shales and rarely siliceous rocks) of the Takyr suite, $D_3$-$C_1$

Irtysh complex gabbro

Kystav-Kurchum formation rocks, represented by schist and granite-gneisses, blastomilonites along them with dikes of the Irtysh complex cataclasite gabbro (green)

Kystav-Kurchum formation rocks, represented by green schist rocks

Zone of the main shear, filled with green schists

Quaternary deposits

Isoclinal folding of the northwestern strike

Faults: a)strike-slip, b) thrust

Section line A-B

Irtysh river

Main roads

thrust;

Ust-Kamenogorsk sity boundary

**Figure 3.** The scheme of the geological structure of the Irtysh shear zone in the area of Ust-Kamenogorsk.

At the base of the thrust (Figure 3), there is a zone in which biotite–muscovite shales include lenticular boudins of cataclastyc gabbro. They are jointly crushed into isoclinal folds. Structurally, blastomylonites, crystalline schists, and gneisses of metapelite composition (biotite, garnet–biotite, biotite–garnet–sillimanite) and granite–gneisses of the Chechek metamorphic complex are located below the Surov massif. The complex is deformed into dome-shaped folds and pushed over sedimentary rocks of the Takyr formation. In the upper part of the metamorphic complex, there are spherical gabbro blocks with a diameter of several meters, in the lower part, there are tectonic lenses of metasedimentary rocks, Kystav–Kurchum Fms.

The thickness of the tectonic lenses reaches 1–2 m, the length is several meters (Figure 4). Figure 4a shows the general appearance of the tectonic mélange. The matrix is represented by granite gneisses, which include oval blocks of quartz–biotite, garnet–biotite, and quartz–biotite–garnet–sillimanite schists of various sizes (up to 70 cm).




**Figure 4.** Photographs of the base of a tectonic mélange represented by granite–gneisses with blocks of metasedimentary rocks: (**a**)—general view, (**b**)—block of metasedimentary rocks, length and height about 1 m, (**c**)—block of metasedimentary rocks (length two meters, height 80 cm), (**d**)—block of metasedimentary rocks (length three meters, height one meter). Coordinates of the observation point in the road recess: 49°52′20.85″ S, 82°37′46.20″ N. See text for description.

In Figure 4b, among the granite gneisses, there is a block of rhythmically layered rocks, the width and height of which are about 80 cm. The layering in the block is oriented at a right angle to the strike of the metamorphic schistosity in the granite gneisses. It is expressed by the alternation of quartz–biotite (quartz sandstones), biotite, and siliceous layers, which form a rhythmic alternation. The thickness of grey and light green siliceous rocks and grey quartz–biotite interlayers is from a few mm to several cm. Figure 4c

shows isoclinal folding in granite–gneisses, including blocks of quartz–biotite and siliceous rocks. Black biotite zones are clearly visible in granite–gneisses. The amplitude of isoclinal folding is about 30 cm, the subsidence of axial planes is consistent with the general sink of granite–gneisses to the northeast, the subsidence angle is 45°. Figure 4d shows a large block of metasedimentary rocks 3 m long and 1 m high. It is represented by alternating quartz–biotite, biotite, and siliceous interlayers. The rocks are intersected by a quartz vein, which creates the appearance of a recumbent fold. Metasedimentary rocks subside to the north-northeast at an angle of 40°.

The metamorphic rocks of the Chechek complex, taking into account the superimposed dome-shaped folding, are characterized by a gentle northeastern immersion of the axial planes of the drawing folds and mineral linearity in metamorphic rocks. Its thickness is estimated at 1200 m. In general, the metamorphic rocks of the Chechek complex and Surov gabbro should be considered as a tectonic mélange formed by the framing of a large gabbro body intruded in the thrust. The southern cataclased gabbro contact with metamorphic rocks sinks to the north at angles of 40–50°, and the eastern and western contacts are gently sloping to the northeast-east. In places, hot contacts of gabbro and metamorphic rocks have been preserved [61,65,68,69].

Tectonically, above the massive gabbro on the right bank of the Irtysh River, there are also metamorphic rocks (mainly blastomylonites in crystalline shales and granite–gneisses), including bodies of gabbro cataclasite up to the first meters in size. Even higher are the metamorphic rocks of the green schist facies of metamorphism, formed by middle Devonian sedimentary rocks (Kystav–Kurchum Fms.). They are characterized by frequent interlayers of siliceous rocks and the mineral linearity of muscovite, manifested along the planes of axial cleavage. The layers are often crumpled into shallow recumbent folds with axial planes and mineral linearity sinking to the northeast and east with angles of 35–10°.

First of all, they often manifest themselves in Z-shaped folds with vertically plunging hinges. The folds are formed in narrow fault zones represented by green schist, mylonites, and blastomylonites from the rocks of the Irtysh metamorphic complex of the epidote amphibolite facies of metamorphism.

The metamorphic shear rocks are most fully represented along the northeastern border of the ISZ on the border with the Rudny Altai terrane (Figures 2 and 3). In the frontal part of the thrust, the granitoids of the Kalba–Narym batholith are located, embedded in the middle Devonian sedimentary rocks (Kystav–Kurchum Fms.) (Figure 2).

### *4.2. The $^{40}Ar/^{39}Ar$ Dating*

In the $^{40}Ar/^{39}Ar$ spectra of almost all analyzed mineral fractions (Table A1, Figure 5), an age plateau is distinguished. In the high-temperature part of the spectra of biotites X-1041 (leucogranite of the Voylochev massif), X-1042 (granite of the Chernovin massif), and X-1047 (granodiorite of the Kurchum massif), a plateau of three or more successive stages is observed, the proportion of which is less than the accepted value of 60% of the $^{39}Ar$ released.

A summary of the thermochronological data we obtained, as well as those obtained earlier, is shown in Figure 2 and in Table 1.

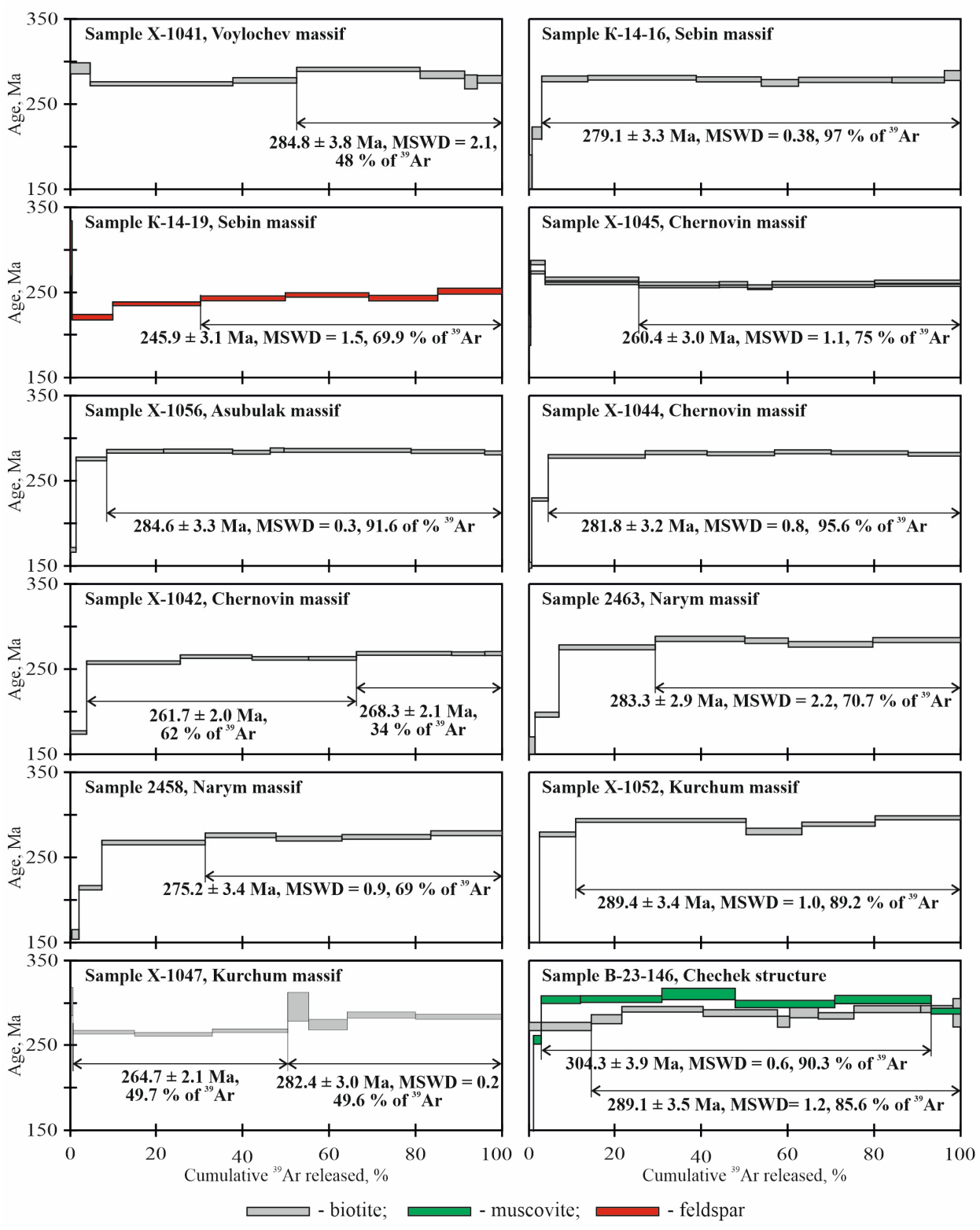


**Figure 5.** $^{40}Ar/^{39}Ar$ age spectra.

## 5. Discussion

### *5.1. Ar/39Ar Dating*

In cases where a high-temperature plateau of three or more successive stages is observed, and the proportion of which is less than the accepted value of 60% of the $^{39}Ar$ released (biotite samples X-1041, X-1042, X-1047), the value of the high-temperature plateau corresponds to the age of closure of the isotope system of the mineral, and the presence of

a plateau in the low-temperature part indicates a complex thermal history of the rock. This may be due to prolonged cooling or superimposed heating. The reason for this heating could be the belts of "postbatolite" dikes (age 286–267 Ma) attributed to the Mirolyubov complex (Figure 2) [5].

When comparing the obtained and published age data for the granitoid complexes of the Kalba–Narym batholith and the Chechek metamorphic complex, it can be noted (Table 1, Figure 2) that for each of the studied objects, the measured age correlates with the stability of isotope systems, decreasing in the series U/Pb for zircon → $^{40}Ar/^{39}Ar$ for muscovite → $^{40}Ar/^{39}Ar$ for biotite → $^{40}Ar/^{39}Ar$ for feldspar → AFT dating. This sequence is an independent confirmation of the assumption that the $^{40}Ar/^{39}Ar$ datings obtained correspond to the closing time of their K/Ar isotope system [55].

### *5.2. Thermochronology*

The totality of all the dates measured by us and taken from the literature, shown in Table 1, is used in the thermochronological diagram (Figure 6). Each dating corresponds to the value of the closing temperature of the isotope system ($T_c$) or the formation ($T_f$) of the rocks as a whole in the case of U/Pb dating by zircon.

The formation of metamorphic rocks of the Chechek structure was simultaneous with the introduction of the Gabbro–Surov massif (see the geological description in part 2 of the article) [61]. This is confirmed by isotope dating data (Table 1, Figure 2). For muscovite from the Chechek metamorphic complex, an age of 312 ± 3 Ma was obtained by the $^{40}Ar/^{39}Ar$ method [65], consistent with the age of gabbro (313 ± 1 Ma [61]). At the same time, estimates of the conditions of metamorphism of samples taken at various sites of the structure are T = 665–720 °C, P = 4–6 kbar [65]. This corresponds to depths of 13–20 km, with an average of 16 km.

A close age (304 ± 4 Ma) was obtained for muscovite from the tectonic mélange zone at the southwestern contact of the rocks of the Surov gabbro massif (Figure 2a). The closure of the biotite isotope system from the same sample at 289 ± 3 Ma occurred 15 Myr later. To explain the sequential closure of isotopic systems of rocks formed at a depth of 13–20 km, one assumption about the establishment of thermal equilibrium is not enough. It is logical to assume that after its formation, the rocks of the Chechek structure experienced exhumation with an amplitude of several kilometers in the process of moving along the thrust (Figures 2 and 3). Assuming that the amplitude was ~5 km in 23 Myr, this corresponds to a velocity of more than 0.2 mm/year, which confirms the tectonic nature of exhumation.

Indeed, a fairly rapid rise with an erosion rate significantly exceeding 0.33 mm/year could be caused by intense tectonic processes, as we assume, associated with the formation of a cover-thrust structure. For example, a study of the denudation rate of the Longmen Shan Ridge [73], located on the eastern edge of the Tibetan Plateau and characterized by steep terrain and a rate of horizontal contraction of up to 3 mm/year, derived denudation rates from 0.15 to 0.5 mm/year. The highest rates of exhumation and denudation are localized in the hanging walls of large thrusts (Figures 2 and 8 in [73]), emphasizing the role of tectonic structures in regulating the nature of denudation and topography throughout the Longmen Shan range.

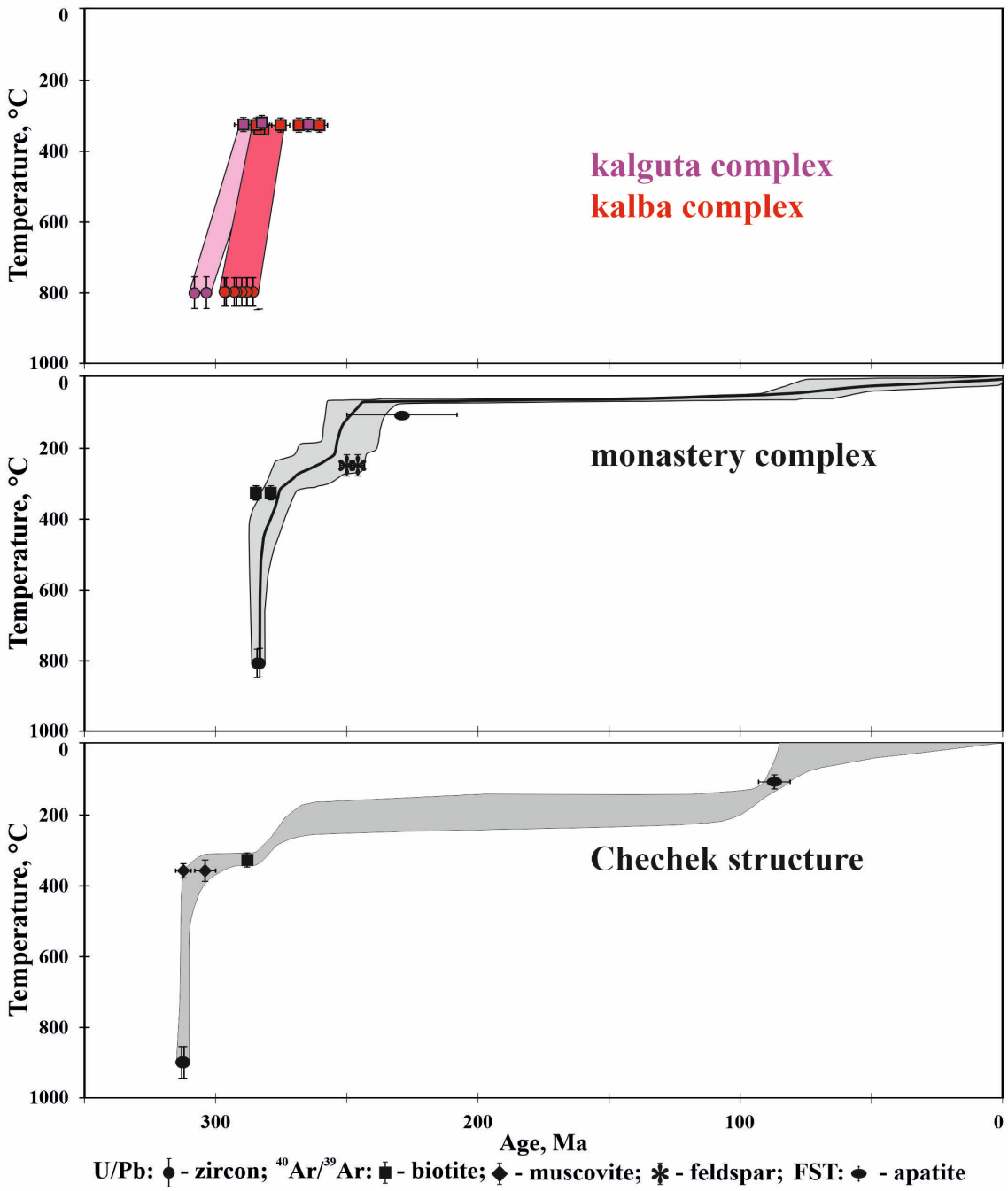


**Figure 6.** Thermochronological history of the Kalba–Narym Batholith granitoids and Chechek structure. The points corresponding to the Kalgutin complex (cherry), the Kalba complex (red) are highlighted in color. The sources of the dates are given in Table 1.

In the history of the Chechek structure, after the closure of the biotite isotope system (289 ± 3 Ma), there is a break of 200 Ma (Table 1, Figures 2 and 6), which ended with the closure of the AFT system from granite gneiss 87 ± 6 Ma ago [17]. Similar values of the AFT age are also observed in the southern extension of the ISZ for granitoid samples—72 ± 4 and 94 ± 4 Ma (Figure 2) [17].

The granitoid massifs of the Kalgutin, Kalba, and Monastery complexes were formed in the early Permian (297–286 Ma). Closure of the biotite isotope system in them (Chernovin, Asubulak, Narym, Sebin massifs, Figures 2a and 6) occurred in a narrow age range of 289–279 Ma. For individual samples, an intermediate plateau with an age of 261–265 Ma is recorded in the low-temperature part of the spectrum. As noted above, this can be

explained by the thermal effect of the dikes of the Mirolyubov complex on the isotope system of biotite.

Thus, it can be noted that for the massifs of granitoid complexes of the Kalba terrane, which were formed in the range of 308–284 Ma, the closure of the biotite isotope system occurs in a narrow age range—289–279 Ma. This can be explained by thermal equilibration after the formation of the massifs occurred at a shallow depth of 5–12 km. Although, given the elongated shape of the granitoid massifs in the north-west direction and the wide manifestation of thrust structures (Figure 2), it is possible to assume the closure of the biotite isotope system during tectonic exhumation.

$^{40}Ar/^{39}Ar$ dating by feldspar (246 ± 3 Ma) from leucogranite in the central part of the Sebin massif is 33 Ma younger, and AFT dating (229 ± 21 Ma [70]) is 50 Ma younger than the age of massif formation.

The observed sequence of closure of low-temperature isotope systems for samples of the Sebin massif is radically different from the sequence observed for the Chechek structure (Figure 6). For the latter, the closure of the AFT system occurred 87 ± 6 Ma ago, 226 Ma after its formation, which may well be explained by gradual exhumation due to erosive denudation. At the same time, the closure of the AFT system in the 3 samples of leukogranites of the Sebin massif occurred much earlier. We believe that the tectonic nature of the exhumation of the Sebin massif should be used to explain this difference. We assume thrust motion as a probable exhumation mechanism (Figure 2b).

### *5.3. Geological Implications*

The evolution of the CAFB includes a long history of the formation of late Neoproterozoic–Paleozoic orogens along the border of the Siberian continent. In the late Paleozoic, the closure of oceanic basins and the collision of the Eastern European and Siberian continents occurred. The process of tectonic transition from subduction to collision in this vast territory, characterized by the formation of cover-thrust and shear structures, is still poorly understood, with the exception, perhaps, of the Chinese Altai Orogen.

The Chinese Altai orogen is a continuation to the south of the Gorny–Altai terrane. The East-West Junggarian terrane is a continuation to the south of the Kalba–Narym terrane. The southeastern extension of the ISZ is the border between the Chinese Altai orogen and the East-West Junggarian terrane (Figure 1). In the Chinese Altai orogen, a variety of publications [34,36,74] prove the late Paleozoic transition from subduction to late Carboniferous collisional high-temperature metamorphism and early Permian granite magmatism [75,76]. It was revealed [36] that in the late Carboniferous (322–295 Ma) there was a thickening of the orogen, the formation of thrust and high-temperature collision metamorphism, including the ISZ, associated with the collision of the Chinese Altai orogen with the East Junggarian terrane within the NE-SW compression. Then there was a stretching of the orogen (295–283 Ma), which could be responsible for the high thermal gradient and the development of widespread early Permian magmatism. It was followed by a transpression event (folding and lateral strike-slip) (283–253 Ma) associated with the oblique convergence of the Chinese Altai orogen with the Eastern Junggarian terrane through the ISZ. It is recorded by $^{40}Ar/^{39}Ar$ dating of syn-strike-slip hornblende and biotite [35,77].

For the AACS, we have obtained new geological and geochronological data that support a scenario similar to the Chinese Altai orogen and well support the manifestation of late Carboniferous–early Permian cover-thrust tectonics and related manifestations of magmatism (Kalba–Narym batholith) and metamorphism within the ISZ. It is shown that in the area of Ust'-Kamenogorsk, the late Carboniferous Surov gabbro complex and Chechek metamorphic rocks are located in a cover-thrust structure deformed into dome-shaped folds. It was formed as a result of the general NE-SW compression, which is also

characteristic of the Chinese Altai. Metamorphic rocks form a tectonic mélange by the framing of a large hot gabbro body embedded in the thrust structure. Tectonically higher are the metamorphic rocks of the green schist facies of metamorphism, formed by middle Devonian sedimentary rocks (Kystav–Kurchum Fms.). They are characterized by shallow recumbent folds with axial planes and mineral linearity sinking to the northeast and east at angles of 35–10°, which also indicates a regional NE–SW compression of the region. As a result of the formation of the cover-thrust structure, volcanogenic sedimentary and sedimentary rocks of the AACS are everywhere compressed, close to isoclinal folds of the northwestern strike of axial planes inclined also to the northeast and east [2,10].

The ISZ is located between the late Silurian–early Carboniferous formations of the Altai active margin (Rudny–Altai terrane) and the Middle Devonian–early Carboniferous turbidites of the pre-arc trough (Kalba–Narym terrane) and probably represents a fragment of the transition zone from subduction to collision, limited by strike-slip. Lateral strike-slip displacements within the studied region are manifested in Z-shaped folds with vertically sinking hinges formed in narrow fault zones represented by green schist, mylonites, and blastomylonites from rocks of the Chechek metamorphic complex of the epidote-amphibolite facies of metamorphism. Lateral strike-slip displacements are most fully developed on the border of the ISZ with the Rudny–Altai terrane and are an object for further detailed study.

The thermochronological reconstruction (Figure 6) carried out for the Chechek metamorphic rocks and the Kalba–Narym batholith indicates the manifestation of a large late Carboniferous–Middle Triassic (312–229 Ma) tectonic stage, as a result of which the rocks were eroded and brought to the surface. Thus, the Chechek metamorphic rocks characterizing the zone of complete tectonic mélange in the late Carboniferous–early Permian (312–289 Ma) were brought to the surface at a denudation rate of >0.2 mm/year. The most complete set of dates obtained by various methods characterizes the leucogranites of the Sebin massif of the monastery complex of the Kalba–Narym batholith. It was found that if based on the results of $^{40}Ar/^{39}Ar$ dating of feldspar and AFT dating, in the range of at least 250–230 Ma years ago, the leucogranites of the massif experienced an tectonic exhumation during thrust motion.

## 6. Conclusions

As a result of new geological and geochronological data with thermochronological interpretation, the sequence of the AACS formation stages in the Kalba–Narym terrane has been established:

1. At an early stage in the Carboniferous–early Permian (312–289 Ma), the ISZ formed as a shallow thrust structure under conditions of NE–SW compression. Synchronously with the thrust, the intrusion of the gabbro of the Irtysh complex (Surov massif and others) and the formation of tectonic mélange with gabbro-cataclasites and metamorphic rocks occurred. The foundation of the Chechek dome structure corresponds to this stage.
2. At the next stage, the formation of a cover-thrust structure involving turbidites of the Middle Devonian–early Carboniferous (Kalba–Narym terrane) led to melting at the middle levels of the thickened crust and the formation of the early Permian Kalba–Narym batholith (297–284 Ma).
3. Rapid denudation of the created orogen occurred at the final stage of collapse until the Early Triassic (279–229 Ma).

Thus, in contrast to the currently prevailing ideas about the significant role of strike-slip tectonics, thrust and cover-thrust processes played a key role at almost all stages of the formation and evolution of the AACS. The Irtysh Shear Zone is located between

the late Silurian–early Carboniferous formations of the Altai active margin (Rudny–Altai terrane) and the Middle Devonian–early Carboniferous turbidites of the pre-arc trough (Kalba–Narym terrane) and is probably a result of the subduction zone processes, followed by collisional processes, and only then—strike-slip processes.

**Author Contributions:** Writing an article, preparation of drawings, literary review, study of the Chechek granite–gneiss structure and sampling—A.T. and M.B.; study of magmatic complexes of the Kalba–Narym terrane and the Chechek granite–gneiss structure, sampling, participation in the writing of the article—S.V.K. and P.K.; participation in the field work, discussion and writing of the article—V.K.; the study of the Sebin massif of the monastery complex, sampling, $^{40}Ar/^{39}Ar$ dating, thermochronological interpretation of the data obtained, participation in the writing of the article—N.M.; study of the Chechek granite–gneiss structure, selection, study of samples and preparation for $^{40}Ar/^{39}Ar$ dating, participation in the preparation of the article—V.D.Z. All authors have read and agreed to the published version of the manuscript.

**Funding:** The study was supported by the Russian Science Foundation (grant No. 22-17-00038, thermochronology) and was carried out on government assignment to the V.S. Sobolev Institute of Geology and Mineralogy (Projects No. 122041400057-2 and No. 122041400071-5) and Ministry of Science and Higher Education of the Republic of Kazakhstan (Program IRN BR21882301).

**Data Availability Statement:** The original contributions presented in this study are included in the article. Further inquiries can be directed to the corresponding author.

**Conflicts of Interest:** The authors declare no conflicts of interest.

## Appendix A

**Table A1.** $^{40}Ar/^{39}Ar$ data for minerals from the samples of the Kalba–Narym batholith and the Chechek granite–gneiss structure.

| T °C | $^{40}Ar$ ($cm^3$ STP) | $^{40}Ar/^{39}Ar \pm 1\sigma$ | $^{38}Ar/^{39}Ar \pm 1\sigma$ | $^{37}Ar/^{39}Ar \pm 1\sigma$ | $^{36}Ar/^{39}Ar \pm 1\sigma$ | Ca/K | $\sum^{39}Ar$ (%) | Age (Ma) $\pm 1\sigma$ | $^{40}Ar$ * (%) |
|---|---|---|---|---|---|---|---|---|---|
| Sample X-1041 biotite, weight 4.95 mg, J = 0.004528 ± 0.000054 [1], plateau age (850–1100 °C) = 284.8 ± 3.8 Ma (1σ) | | | | | | | | | |
| 500 | 390.5 | 57.3 ± 0.3 | 0.01922 ± 0.00520 | 0.00002 ± 0.00002 | 0.00021 ± 0.00436 | 0.0001 | 4.6 | 291.7 ± 6.6 | 99.9 |
| 650 | 2617.0 | 53.4 ± 0.1 | 0.00770 ± 0.00035 | 0.00008 ± 0.00003 | 0.00001 ± 0.00083 | 0.0003 | 37.6 | 273.5 ± 2.4 | 100.0 |
| 750 | 1191.1 | 54.2 ± 0.1 | 0.01199 ± 0.00168 | 0.04209 ± 0.00460 | 0.00001 ± 0.00169 | 0.1515 | 52.4 | 277.6 ± 3.2 | 100.0 |
| 850 | 2415.3 | 57.0 ± 0.1 | 0.00001 ± 0.00035 | 0.00026 ± 0.00250 | 0.00001 ± 0.00069 | 0.0009 | 81.0 | 290.6 ± 2.4 | 100.0 |
| 950 | 853.8 | 55.7 ± 0.2 | 0.00523 ± 0.00211 | 0.00009 ± 0.00007 | 0.00014 ± 0.00272 | 0.0003 | 91.3 | 284.2 ± 4.4 | 99.9 |
| 1025 | 234.8 | 54.0 ± 0.3 | 0.00049 ± 0.00007 | 0.00027 ± 0.00031 | 0.00044 ± 0.00554 | 0.0010 | 94.3 | 275.8 ± 8.2 | 99.8 |
| 1100 | 461.2 | 54.3 ± 0.1 | 0.00826 ± 0.00263 | 0.00107 ± 0.00002 | 0.00033 ± 0.00149 | 0.0039 | 100.0 | 277.4 ± 3.0 | 99.8 |
| Sample KA-14-16 biotite, weight 52.01 mg, J = 0.004528 ± 0.000054 [1], plateau age (720–1130 °C) = 279.1 ± 3.3 Ma (1σ) | | | | | | | | | |
| 500 | 22.5 | 43.8 ± 0.7 | 0.05938 ± 0.02329 | 16.63285 ± 7.78847 | 0.06168 ± 0.01523 | 59.9 | 0.7 | 162.8 ± 27.5 | 58.4 |
| 610 | 97.2 | 59.8 ± 0.3 | 0.05926 ± 0.00630 | 3.99485 ± 2.93448 | 0.08588 ± 0.00393 | 14.4 | 3.0 | 216.0 ± 7.2 | 57.6 |
| 720 | 371.4 | 48.0 ± 0.1 | 0.01561 ± 0.00161 | 1.73254 ± 0.60034 | 0.00884 ± 0.00130 | 6.3 | 13.6 | 279.6 ± 3.4 | 94.6 |
| 800 | 844.9 | 46.4 ± 0.1 | 0.01708 ± 0.00025 | 0.01537 ± 0.15000 | 0.00280 ± 0.00051 | 0.1 | 38.8 | 280.9 ± 2.7 | 98.2 |
| 850 | 509.1 | 46.7 ± 0.1 | 0.01585 ± 0.00100 | 0.14254 ± 0.38051 | 0.00485 ± 0.00090 | 0.5 | 53.8 | 279.1 ± 3.0 | 96.9 |
| 920 | 296.8 | 47.4 ± 0.1 | 0.02001 ± 0.00191 | 1.82078 ± 1.74010 | 0.00974 ± 0.00179 | 6.5 | 62.4 | 274.9 ± 3.9 | 93.9 |
| 1020 | 730.9 | 46.6 ± 0.1 | 0.01493 ± 0.00108 | 0.02376 ± 0.30843 | 0.00487 ± 0.00091 | 0.1 | 84.1 | 278.5 ± 3.0 | 96.9 |
| 1080 | 416.8 | 47.3 ± 0.1 | 0.01827 ± 0.00208 | 2.03645 ± 0.75456 | 0.00751 ± 0.00130 | 7.3 | 96.2 | 278.2 ± 3.4 | 95.3 |
| 1130 | 131.2 | 48.0 ± 0.1 | 0.01356 ± 0.00322 | 3.15342 ± 1.56345 | 0.00651 ± 0.00311 | 11.3 | 100.0 | 283.6 ± 5.9 | 96.0 |
| Sample KA-14-19 feldspar, weight 125.67 mg, J = 0.004528 ± 0.000054 [1], plateau age (825–1130 °C) = 245.9 ± 3.1 Ma (1σ) | | | | | | | | | |
| 500 | 16.9 | 65.7 ± 1.7 | 0.02802 ± 0.02545 | 1.26424 ± 3.96484 | 0.05341 ± 0.01919 | 4.5 | 0.4 | 301.8 ± 32.4 | 76.0 |
| 625 | 240.2 | 40.0 ± 0.1 | 0.01436 ± 0.00227 | 0.56055 ± 0.24672 | 0.01465 ± 0.00147 | 2.0 | 9.8 | 220.7 ± 3.2 | 89.2 |
| 725 | 524.4 | 40.4 ± 0.1 | 0.01805 ± 0.00072 | 0.40446 ± 0.24077 | 0.00672 ± 0.00034 | 1.5 | 30.1 | 236.5 ± 2.2 | 95.1 |
| 825 | 517.4 | 41.2 ± 0.1 | 0.01845 ± 0.00062 | 0.35746 ± 0.18756 | 0.00590 ± 0.00109 | 1.3 | 49.8 | 243.0 ± 2.9 | 95.8 |
| 925 | 515.0 | 41.7 ± 0.1 | 0.01629 ± 0.00125 | 0.31492 ± 0.28741 | 0.00517 ± 0.00078 | 1.1 | 69.1 | 246.9 ± 2.6 | 96.3 |
| 1025 | 429.3 | 42.0 ± 0.1 | 0.01733 ± 0.00101 | 0.69472 ± 0.04437 | 0.00849 ± 0.00136 | 2.5 | 85.1 | 243.2 ± 3.2 | 94.0 |
| 1130 | 405.6 | 42.7 ± 0.1 | 0.01868 ± 0.00158 | 1.80304 ± 0.54957 | 0.00575 ± 0.00157 | 6.5 | 100.0 | 251.4 ± 3.5 | 96.0 |

**Table A1.** *Cont.*

| T °C | $^{40}$Ar (cm$^3$ STP) | $^{40}$Ar/$^{39}$Ar ± 1σ | $^{38}$Ar/$^{39}$Ar ± 1σ | $^{37}$Ar/$^{39}$Ar ± 1σ | $^{36}$Ar/$^{39}$Ar ± 1σ | Ca/K | $\sum^{39}$Ar (%) | Age (Ma) ± 1σ | $^{40}$Ar * (%) |
|---|---|---|---|---|---|---|---|---|---|
| Sample X-1045 biotite, weight 9.86 mg, J = 0.004528 ± 0.000054 [1], plateau age (750–1100 °C) = 260.4 ± 3.0 Ma (1σ) | | | | | | | | | |
| 500 | 91.0 | 45.9 ± 0.3 | 0.06044 ± 0.01423 | 3.80707 ± 0.18499 | 0.02491 ± 0.00748 | 13.70 | 0.4 | 198.8 ± 11.0 | 84.0 |
| 600 | 965.2 | 55.2 ± 0.1 | 0.02026 ± 0.00145 | 0.25325 ± 0.02180 | 0.00471 ± 0.00109 | 0.91 | 3.7 | 285.2 ± 2.6 | 97.5 |
| 700 | 6005.1 | 53.1 ± 0.1 | 0.01943 ± 0.00024 | 0.03393 ± 0.00338 | 0.00196 ± 0.00053 | 0.12 | 25.4 | 266.0 ± 2.1 | 98.9 |
| 750 | 5037.7 | 51.8 ± 0.1 | 0.01511 ± 0.00008 | 0.01110 ± 0.00074 | 0.00174 ± 0.00058 | 0.04 | 44.1 | 260.3 ± 2.1 | 99.0 |
| 800 | 1765.3 | 51.7 ± 0.1 | 0.01582 ± 0.00033 | 0.00828 ± 0.00220 | 0.00083 ± 0.00035 | 0.03 | 50.6 | 260.9 ± 2.0 | 99.5 |
| 900 | 1522.2 | 51.4 ± 0.1 | 0.01543 ± 0.00024 | 0.02381 ± 0.00194 | 0.00268 ± 0.00046 | 0.09 | 56.3 | 257.1 ± 2.0 | 98.5 |
| 1025 | 6418.3 | 51.9 ± 0.1 | 0.01449 ± 0.00008 | 0.00698 ± 0.00046 | 0.00123 ± 0.00054 | 0.02 | 80.1 | 261.2 ± 2.1 | 99.3 |
| 1100 | 5418.4 | 52.1 ± 0.1 | 0.01400 ± 0.00009 | 0.00207 ± 0.00067 | 0.00106 ± 0.00031 | 0.01 | 100.0 | 262.6 ± 2.0 | 99.4 |
| Sample X-1056 biotite, weight 71.5 mg, J = 0.004528 ± 0.000054 [1], plateau age (650–1130 °C) = 284.6 ± 3.3 Ma (1σ) | | | | | | | | | |
| 500 | 71.2 | 42.3 ± 0.1 | 0.02143 ± 0.00369 | 0.14170 ± 0.01263 | 0.03549 ± 0.00165 | 0.51 | 1.3 | 169.0 ± 2.8 | 75.2 |
| 600 | 531.1 | 58.4 ± 0.1 | 0.01791 ± 0.00040 | 0.02686 ± 0.00165 | 0.01668 ± 0.00036 | 0.10 | 8.4 | 275.7 ± 2.1 | 91.6 |
| 650 | 961.7 | 56.8 ± 0.1 | 0.01561 ± 0.00020 | 0.00895 ± 0.00096 | 0.00504 ± 0.00026 | 0.03 | 21.6 | 284.7 ± 2.2 | 97.4 |
| 700 | 1151.4 | 56.1 ± 0.1 | 0.01555 ± 0.00018 | 0.00523 ± 0.00080 | 0.00246 ± 0.00023 | 0.02 | 37.6 | 285.1 ± 2.2 | 98.7 |
| 750 | 623.5 | 55.7 ± 0.1 | 0.01624 ± 0.00013 | 0.01362 ± 0.00144 | 0.00220 ± 0.00056 | 0.05 | 46.3 | 283.5 ± 2.3 | 98.8 |
| 850 | 229.2 | 55.9 ± 0.1 | 0.01740 ± 0.00110 | 0.02538 ± 0.00314 | 0.00093 ± 0.00096 | 0.09 | 49.5 | 286.1 ± 2.5 | 99.5 |
| 975 | 2125.4 | 56.2 ± 0.1 | 0.01544 ± 0.00008 | 0.01527 ± 0.00029 | 0.00235 ± 0.00025 | 0.05 | 78.9 | 285.7 ± 2.2 | 98.8 |
| 1050 | 1223.3 | 55.9 ± 0.1 | 0.01539 ± 0.00019 | 0.03660 ± 0.00062 | 0.00218 ± 0.00032 | 0.13 | 96.0 | 284.4 ± 2.2 | 98.9 |
| 1130 | 288.9 | 56.0 ± 0.1 | 0.01608 ± 0.00041 | 0.15098 ± 0.00084 | 0.00354 ± 0.00061 | 0.54 | 100.0 | 282.7 ± 2.3 | 98.1 |
| Sample X-1044 biotite, weight 71.5 mg, J = 0.004528 ± 0.000054 [1], plateau age (650–1130 °C) = 284.6 ± 3.3 Ma (1σ) | | | | | | | | | |
| 500 | 19.0 | 39.2 ± 0.2 | 0.02941 ± 0.00265 | 0.40784 ± 0.01722 | 0.03673 ± 0.00212 | 1.47 | 0.6 | 150.7 ± 3.5 | 72.3 |
| 600 | 140.4 | 49.1 ± 0.1 | 0.01934 ± 0.00098 | 0.09718 ± 0.00144 | 0.01826 ± 0.00049 | 0.35 | 4.4 | 227.9 ± 1.9 | 89.0 |
| 700 | 934.6 | 55.3 ± 0.1 | 0.01565 ± 0.00017 | 0.02390 ± 0.00042 | 0.00370 ± 0.00018 | 0.09 | 26.9 | 278.5 ± 2.1 | 98.0 |
| 775 | 599.7 | 55.7 ± 0.1 | 0.01575 ± 0.00028 | 0.01383 ± 0.00187 | 0.00173 ± 0.00053 | 0.05 | 41.2 | 282.9 ± 2.3 | 99.1 |
| 875 | 658.0 | 56.0 ± 0.1 | 0.01646 ± 0.00041 | 0.03710 ± 0.00134 | 0.00374 ± 0.00039 | 0.13 | 56.9 | 281.6 ± 2.2 | 98.0 |
| 975 | 554.3 | 56.2 ± 0.1 | 0.01502 ± 0.00032 | 0.04986 ± 0.00169 | 0.00263 ± 0.00030 | 0.18 | 70.0 | 284.0 ± 2.2 | 98.6 |
| 1050 | 749.2 | 55.9 ± 0.1 | 0.01536 ± 0.00033 | 0.07133 ± 0.00117 | 0.00257 ± 0.00016 | 0.26 | 87.8 | 282.8 ± 2.1 | 98.6 |
| 1130 | 512.0 | 56.0 ± 0.1 | 0.01504 ± 0.00023 | 0.19017 ± 0.00162 | 0.00416 ± 0.00035 | 0.68 | 100.0 | 281.0 ± 2.2 | 97.8 |
| Sample X-1042 biotite, weight 5.81 mg, J = 0.004528 ± 0.000054 [1], plateau age (900–1100 °C) = 268.3 ± 2.1 Ma (1σ) | | | | | | | | | |
| 500 | 500.0 | 40.8 ± 0.1 | 0.02330 ± 0.00072 | 0.03415 ± 0.00579 | 0.02496 ± 0.00101 | 0.12 | 3.8 | 175.4 ± 2.0 | 81.9 |
| 600 | 3636.3 | 51.4 ± 0.1 | 0.01567 ± 0.00013 | 0.00354 ± 0.00103 | 0.00405 ± 0.00027 | 0.01 | 25.5 | 257.6 ± 2.0 | 97.7 |
| 675 | 2827.7 | 52.2 ± 0.1 | 0.01543 ± 0.00016 | 0.00801 ± 0.00123 | 0.00160 ± 0.00049 | 0.03 | 42.1 | 264.6 ± 2.1 | 99.1 |
| 800 | 2231.2 | 52.3 ± 0.1 | 0.01390 ± 0.00019 | 0.01403 ± 0.00131 | 0.00352 ± 0.00030 | 0.05 | 55.2 | 262.6 ± 2.0 | 98.0 |
| 900 | 1910.8 | 53.0 ± 0.1 | 0.01665 ± 0.00019 | 0.01726 ± 0.00161 | 0.00566 ± 0.00048 | 0.06 | 66.3 | 262.6 ± 2.1 | 96.8 |
| 1000 | 3810.1 | 53.0 ± 0.1 | 0.01522 ± 0.00012 | 0.01699 ± 0.00119 | 0.00161 ± 0.00053 | 0.06 | 88.3 | 268.5 ± 2.2 | 99.1 |
| 1050 | 1336.5 | 53.3 ± 0.1 | 0.01608 ± 0.00029 | 0.04024 ± 0.00315 | 0.00296 ± 0.00036 | 0.14 | 96.0 | 268.2 ± 2.1 | 98.4 |
| 1100 | 698.2 | 53.8 ± 0.1 | 0.02001 ± 0.00074 | 0.20121 ± 0.00596 | 0.00454 ± 0.00075 | 0.72 | 100.0 | 268.4 ± 2.3 | 97.5 |
| Sample 2463 biotite, weight 21.75mg, J = 0.004528 ± 0.000054 [1], plateau age (900–1130 °C) = 283.3 ± 2.9 Ma (1σ) | | | | | | | | | |
| 500 | 30.0 | 33.3 ± 0.2 | 0.02120 ± 0.02120 | 0.08281 ± 0.01910 | 0.03934 ± 0.00628 | 0.2981 | 1.4 | 157.4 ± 13.0 | 65.2 |
| 600 | 124.5 | 35.0 ± 0.1 | 0.02333 ± 0.02333 | 0.02432 ± 0.00227 | 0.02595 ± 0.00105 | 0.0876 | 7.0 | 196.5 ± 2.9 | 78.2 |
| 700 | 603.9 | 42.3 ± 0.1 | 0.02018 ± 0.02018 | 0.01386 ± 0.00076 | 0.01009 ± 0.00041 | 0.0499 | 29.3 | 275.7 ± 2.9 | 93.0 |
| 800 | 578.4 | 43.5 ± 0.1 | 0.02021 ± 0.02021 | 0.01265 ± 0.00103 | 0.00903 ± 0.00053 | 0.0455 | 50.0 | 285.7 ± 3.1 | 93.9 |
| 900 | 278.7 | 43.2 ± 0.1 | 0.02146 ± 0.02146 | 0.02131 ± 0.00300 | 0.00928 ± 0.00077 | 0.0767 | 60.1 | 283.5 ± 3.2 | 93.7 |
| 1000 | 542.6 | 43.3 ± 0.1 | 0.02125 ± 0.02125 | 0.02368 ± 0.00146 | 0.01160 ± 0.00082 | 0.0852 | 79.6 | 279.2 ± 3.3 | 92.1 |
| 1130 | 564.7 | 43.3 ± 0.1 | 0.01970 ± 0.01970 | 0.07923 ± 0.00085 | 0.00912 ± 0.00028 | 0.2852 | 100.0 | 284.2 ± 2.9 | 93.8 |
| Sample 2458 biotite, weight 39.8 mg, J = 0.004528 ± 0.000054 [1], plateau age (800–1130 °C) = 275.2 ± 3.4 Ma (1σ) | | | | | | | | | |
| 500 | 72.6 | 33.2 ± 0.1 | 0.02810 ± 0.00232 | 0.06164 ± 0.00328 | 0.03617 ± 0.00272 | 0.22 | 1.7 | 159.5 ± 5.7 | 67.8 |
| 600 | 257.9 | 37.1 ± 0.1 | 0.02130 ± 0.00044 | 0.02316 ± 0.00169 | 0.02176 ± 0.00069 | 0.08 | 7.0 | 214.4 ± 2.6 | 82.7 |
| 700 | 1329.7 | 42.3 ± 0.1 | 0.01945 ± 0.00012 | 0.01324 ± 0.00040 | 0.01173 ± 0.00020 | 0.05 | 31.0 | 267.5 ± 2.7 | 91.8 |
| 800 | 939.7 | 43.7 ± 0.1 | 0.01900 ± 0.00022 | 0.01347 ± 0.00059 | 0.01176 ± 0.00020 | 0.05 | 47.5 | 276.0 ± 2.8 | 92.1 |
| 900 | 863.0 | 43.1 ± 0.1 | 0.01906 ± 0.00018 | 0.01866 ± 0.00060 | 0.01204 ± 0.00031 | 0.07 | 62.8 | 272.1 ± 2.8 | 91.8 |
| 1000 | 1175.2 | 43.5 ± 0.1 | 0.01941 ± 0.00014 | 0.01991 ± 0.00042 | 0.01220 ± 0.00009 | 0.07 | 83.4 | 274.2 ± 2.7 | 91.7 |
| 1130 | 954.1 | 44.1 ± 0.1 | 0.01902 ± 0.00023 | 0.11439 ± 0.00069 | 0.01178 ± 0.00026 | 0.41 | 100.0 | 278.5 ± 2.8 | 92.1 |
| Sample X-1052 biotite, weight 3.3 mg, J = 0.004528 ± 0.000054 [1], plateau age (850–1100 °C) = 289.4 ± 3.4 Ma (1σ) | | | | | | | | | |
| 500 | 20.9 | 62.2 ± 1.3 | 0.05037 ± 0.02094 | 0.87014 ± 0.18577 | 0.19526 ± 0.02100 | 3.132 | 0.6 | 24.4 ± 32.6 | 7.4 |
| 600 | 57.1 | 50.7 ± 0.2 | 0.03431 ± 0.00644 | 0.14209 ± 0.06394 | 0.11289 ± 0.00382 | 0.511 | 2.4 | 91.7 ± 5.8 | 34.3 |
| 700 | 294.1 | 58.4 ± 0.1 | 0.02949 ± 0.00139 | 0.05529 ± 0.01259 | 0.01127 ± 0.00136 | 0.199 | 10.8 | 276.5 ± 2.8 | 94.3 |
| 850 | 1430.0 | 60.3 ± 0.1 | 0.01715 ± 0.00023 | 0.02236 ± 0.00224 | 0.00558 ± 0.00032 | 0.080 | 50.3 | 293.0 ± 2.2 | 97.3 |
| 950 | 469.1 | 60.4 ± 0.1 | 0.01869 ± 0.00086 | 0.10875 ± 0.00882 | 0.01643 ± 0.00098 | 0.391 | 63.2 | 278.5 ± 2.5 | 92.0 |
| 950 | 469.1 | 60.4 ± 0.1 | 0.01869 ± 0.00086 | 0.10875 ± 0.00882 | 0.01643 ± 0.00098 | 0.391 | 63.2 | 278.5 ± 2.5 | 92.0 |
| 1025 | 614.1 | 60.2 ± 0.1 | 0.02091 ± 0.00062 | 0.00100 ± 0.00719 | 0.00849 ± 0.00087 | 0.004 | 80.2 | 288.5 ± 2.4 | 95.8 |
| 1100 | 719.8 | 60.4 ± 0.1 | 0.01887 ± 0.00070 | 0.02122 ± 0.00600 | 0.00381 ± 0.00065 | 0.076 | 100.0 | 296.0 ± 2.4 | 98.1 |

**Table A1.** *Cont.*

| T °C | $^{40}$Ar (cm$^3$ STP) | $^{40}$Ar/$^{39}$Ar ± 1σ | $^{38}$Ar/$^{39}$Ar ± 1σ | $^{37}$Ar/$^{39}$Ar ± 1σ | $^{36}$Ar/$^{39}$Ar ± 1σ | Ca/K | $\sum^{39}$Ar (%) | Age (Ma) ± 1σ | $^{40}$Ar * (%) |
|---|---|---|---|---|---|---|---|---|---|
| Sample X-1047 biotite, weight 5.24 mg, J = 0.004528 ± 0.000054 [1], plateau age (800–1100 °C) = 282.4 ± 3.0 Ma (1σ) | | | | | | | | | |
| 500 | 61.3 | 61.8 ± 0.5 | 0.03026 ± 0.00880 | 0.20401 ± 0.03479 | 0.00451 ± 0.01198 | 0.734 | 0.6 | 302.0 ± 16.6 | 97.8 |
| 650 | 1270.7 | 55.0 ± 0.1 | 0.00836 ± 0.00019 | 0.00036 ± 0.00135 | 0.00853 ± 0.00066 | 0.001 | 14.9 | 265.1 ± 2.2 | 95.4 |
| 700 | 1563.9 | 53.6 ± 0.1 | 0.01071 ± 0.00037 | 0.01784 ± 0.00141 | 0.00561 ± 0.00054 | 0.064 | 32.9 | 262.5 ± 2.1 | 96.9 |
| 750 | 1522.4 | 53.7 ± 0.1 | 0.01059 ± 0.00047 | 0.01534 ± 0.00308 | 0.00284 ± 0.00074 | 0.055 | 50.4 | 266.8 ± 2.2 | 98.4 |
| 800 | 501.3 | 63.8 ± 0.4 | 0.09076 ± 0.01452 | 0.00591 ± 0.02531 | 0.01590 ± 0.01223 | 0.021 | 55.2 | 295.9 ± 16.9 | 92.7 |
| 925 | 850.6 | 58.8 ± 0.1 | 0.00911 ± 0.00225 | 0.00423 ± 0.00551 | 0.01633 ± 0.00282 | 0.015 | 64.1 | 272.2 ± 4.4 | 91.8 |
| 1025 | 1485.6 | 58.0 ± 0.2 | 0.00832 ± 0.00177 | 0.00721 ± 0.00663 | 0.00321 ± 0.00213 | 0.026 | 79.9 | 286.1 ± 3.7 | 98.4 |
| 1100 | 1942.4 | 59.8 ± 0.1 | 0.01366 ± 0.00172 | 0.00397 ± 0.00436 | 0.01070 ± 0.00154 | 0.014 | 100.0 | 284.2 ± 3.0 | 94.7 |
| Sample B-23-146 biotite, weight 56.52 mg, J = 0.004528 ± 0.000054 [1], plateau age (540–1130 °C) = 289.1 ± 3.5 Ma (1σ) | | | | | | | | | |
| 500 | 1475.3 | 45.5 ± 0.1 | 0.05481 ± 0.00154 | 0.08531 ± 0.00183 | 0.02000 ± 0.00236 | 0.307 | 14.4 | 272.2 ± 5.3 | 87.0 |
| 540 | 739.0 | 46.4 ± 0.1 | 0.05862 ± 0.00128 | 0.08216 ± 0.00440 | 0.01834 ± 0.00234 | 0.296 | 21.5 | 281.2 ± 5.2 | 88.3 |
| 580 | 2019.2 | 47.7 ± 0.1 | 0.03036 ± 0.00164 | 0.05464 ± 0.00293 | 0.01642 ± 0.00079 | 0.197 | 40.3 | 292.9 ± 3.3 | 89.8 |
| 680 | 1897.9 | 49.0 ± 0.1 | 0.03041 ± 0.00095 | 0.04899 ± 0.00194 | 0.02329 ± 0.00145 | 0.176 | 57.6 | 288.4 ± 4.0 | 86.0 |
| 750 | 329.6 | 51.9 ± 0.2 | 0.06585 ± 0.00199 | 0.14083 ± 0.00598 | 0.03874 ± 0.00306 | 0.507 | 60.4 | 278.3 ± 6.4 | 78.0 |
| 850 | 726.2 | 48.7 ± 0.2 | 0.05198 ± 0.00154 | 0.08909 ± 0.00517 | 0.02158 ± 0.00330 | 0.322 | 67.0 | 289.7 ± 6.9 | 86.9 |
| 950 | 898.5 | 48.3 ± 0.1 | 0.04831 ± 0.00068 | 0.07979 ± 0.00307 | 0.02287 ± 0.00132 | 0.287 | 75.3 | 285.2 ± 3.8 | 86.0 |
| 1050 | 1654.5 | 47.6 ± 0.1 | 0.02852 ± 0.00071 | 0.04228 ± 0.00164 | 0.01602 ± 0.00143 | 0.152 | 90.7 | 293.2 ± 4.0 | 90.1 |
| 1090 | 804.4 | 47.7 ± 0.1 | 0.04002 ± 0.00127 | 0.06076 ± 0.00257 | 0.01650 ± 0.00153 | 0.219 | 98.2 | 293.1 ± 4.1 | 89.8 |
| 1130 | 194.5 | 48.5 ± 0.4 | 0.13083 ± 0.00451 | 0.16040 ± 0.01004 | 0.02136 ± 0.00868 | 0.577 | 100.0 | 288.8 ± 16.6 | 87.0 |
| Sample B-23-146 muscovite, weight 56.52 mg, J = 0.004528 ± 0.000054 [1], plateau age (540–1130 °C) = 289.1 ± 3.5 Ma (1σ) | | | | | | | | | |
| 550 | 58.1 | 70.4 ± 1.0 | 0.07549 ± 0.01069 | 5.97844 ± 0.15611 | 0.19980 ± 0.01286 | 21.522 | 1.0 | 81.0 ± 26.2 | 16.3 |
| 650 | 152.0 | 106.8 ± 0.5 | 0.02627 ± 0.00522 | 0.67446 ± 0.03905 | 0.23315 ± 0.00191 | 2.428 | 2.8 | 256.8 ± 5.0 | 35.6 |
| 750 | 478.5 | 66.7 ± 0.1 | 0.01776 ± 0.00310 | 0.06931 ± 0.03274 | 0.07116 ± 0.00179 | 0.249 | 11.9 | 304.7 ± 4.4 | 68.5 |
| 825 | 906.9 | 60.9 ± 0.1 | 0.01377 ± 0.00175 | 0.05460 ± 0.01719 | 0.05143 ± 0.00134 | 0.197 | 30.8 | 305.3 ± 3.9 | 75.1 |
| 910 | 745.1 | 55.6 ± 0.2 | 0.01799 ± 0.00339 | 0.00549 ± 0.01820 | 0.03006 ± 0.00323 | 0.020 | 47.8 | 311.3 ± 6.7 | 84.0 |
| 985 | 1011.3 | 55.5 ± 0.1 | 0.01475 ± 0.00121 | 0.00360 ± 0.01646 | 0.03622 ± 0.00167 | 0.013 | 70.8 | 299.5 ± 4.3 | 80.7 |
| 1055 | 1123.9 | 63.8 ± 0.1 | 0.01787 ± 0.00388 | 0.00461 ± 0.02962 | 0.06130 ± 0.00205 | 0.017 | 93.2 | 304.8 ± 4.8 | 71.6 |
| 1130 | 377.1 | 69.8 ± 0.1 | 0.02801 ± 0.00591 | 0.02533 ± 0.02013 | 0.08913 ± 0.00095 | 0.091 | 100.0 | 291.2 ± 3.4 | 62.3 |

[1] J—characteristic of the neutron flux during irradiation of samples; *—radiogenic $^{40}$Ar.

## References


1. Zonenshain, L.P.; Kuz'min, M.I.; Natapov, L.M. *Tectonics of the Lithospheric Plates of the USSR Territory*; B.1; Nedra: Moscow, Russia, 1990; 327p. (In Russian)
2. Shcherba, G.N.; Diyachkov, B.A.; Stuchevsky, N.I.; Nakhtigal, G.P.; Antonenko, A.N.; Lubetsky, V.N. Great Altai: Geology and Metallogeny. In *Geological Construction*; Book 1; Gylym: Almaty, Kazakhstan, 1998; 304p. (In Russian)
3. Yelkin, E.A.; Sennikov, N.V.; Buslov, M.M.; Yazikov, A.; Yu Grazianova, R.T.; Bakharev, N.L. Paleogeographic reconstructions of the western part of the Altai-Sayan region in the Ordovician, Silurian and Devonian and their geodynamic interpretation. *Geol. I Geofiz. (Russ. Geol. Geophys.)* **1994**, *35*, 118–145.
4. Buslov, M.M.; Watanabe, T.; Smirnova, L.V.; Fujiwara, Y.; Iwata, K.; De Grave, J.; Semakov, N.N.; Travin, A.V.; Kir'ynova, A.P.; Kokh, D.A. Role of strike-slip faulting in Late Paleozoic–Early Mesozoic tectonics and geodynamics of the Altai–Sayan and East Kazakhstan regions. *Geol. I Geofiz. (Russ. Geol. Geophys.)* **2003**, *44*, 49–75.
5. Khromykh, S.V. Basic and Associated Granitoid Magmatism and Geodynamic Evolution of the Altai Accretion–Collision System (Eastern Kazakhstan). *Russ. Geol. Geophys.* **2022**, *63*, 279–299. [CrossRef]
6. Berzin, N.A.; Dobretsov, N.L. Geodynamic evolution of Southern Siberia in Late Precambrian–Early Paleozoic time. In *Reconstruction of the Paleoasian Ocean*; VSP Int. Sci. Publishers: Leiden, The Netherlands, 1993; pp. 45–62.
7. Mossakovsky, A.A.; Ruzhentsev, S.V.; Samygin, S.G.; Kheraskova, T.N. The Central Asian orogen: Geodynamic evolution and formation history. *Geotektonika* **1993**, *6*, 3–33.
8. Didenko, A.N.; Mossakovsky, A.A.; Pechersky, D.M.; Ruzhentsev, S.V.; Samygin, S.G.; Kheraskova, T.N. Geodynamics of the Paleozoic Oceans of Central Asia. *Geol. I Geofiz. (Russ. Geol. Geophys.)* **1994**, *35*, 59–75.
9. Berzin, N.A.; Coleman, R.G.; Dobretsov, N.L.; Zonenshain, L.P.; Xuchang, X.; Chang, E.Z. Geodynamic map of the western part of the Paleoasian Ocean. *Geol. I Geofiz. (Russ. Geol. Geophys.)* **1994**, *35*, 8–28.
10. Berzin, N.A.; Kungurtsev, L.V. Geodynamic interpretation of Altai– Sayan geological complexes. *Geol. I Geofiz. (Russ. Geol. Geophys.)* **1996**, *37*, 63–81.
11. Dobretsov, N.L. Evolution of structures of the Urals, Kazakhstan, Tien Shan, and Altai–Sayan region within the Ural–Mongolian fold belt (Paleoasian ocean). *Geol. I Geofiz. (Russ. Geol. Geophys.)* **2003**, *44*, 5–28.
12. Ermolov, P.V. *Actual Problems of Isotopic Geology and Metallogeny of Kazakhstan*; Publishing and Printing Center of the Kazakh-Russian University: Karaganda, Kazakhstan, 2013; p. 206. (In Russian)

13. Vladimirov, V.G.; Kruk, N.N.; Khromykh, S.V.; Polyansky, O.P.; Chervov, V.V.; Vladimirov, V.G.; Travin, A.V.; Babin, G.A.; Kuibida, M.L.; Khomyakov, V.D. Permian magmatism and lithospheric deformation in the Altai caused by crustal and mantle thermal processes. *Russ. Geol. Geophys.* **2008**, *49*, 468–479. [CrossRef]
14. Khromykh, S.V.; Kotler, P.D.; Sokolova, E.N. Mantle-crust interaction at the late stage of evolution of Hercynian Altai collision system, Western part of CAOB. *Geodyn. Tectonophys.* **2017**, *8*, 489–493. [CrossRef]
15. Sengör, A.M.C.; Natal'in, B.A.; Burtman, V.S. Evolution of the Altaid tectonic collage and Paleozoic crustal growth in Eurasia. *Nature* **1993**, *36*, 299–307. [CrossRef]
16. Windley, B.F.; Alexeiev, D.; Xiao, W.; Kröner, A.; Badarch, G. Tectonic models for accretion of the Central Asian Orogenic Belt. *J. Geol. Soc. Lond.* **2007**, *164*, 31–47. [CrossRef]
17. Glorie, S.; De Grave, J.; Delvaux, D.; Buslov, M.M.; Zhimulev, F.I.; Vanhaecke, F.; Elburg, M.A.; Van den Haute, P. Tectonic history of the Irtysh shear zone (NE Kazakhstan): New constraints from zircon U/Pb dating, apatite fission track dating and palaeostress analysis. *J. Asian Earth Sci.* **2012**, *45*, 138–149. [CrossRef]
18. Zhang, C.L.; Santosh, M.; Zou, H.B.; Xu, Y.G.; Zhou, G.; Dong, Y.G.; Ding, R.F.; Wang, H.Y. Revisiting the "Irtish tectonic belt": Implications for the Paleozoic tectonic evolution of the Altai orogen. *J. Asian Earth Sci.* **2012**, *52*, 117–133. [CrossRef]
19. Kröner, A.; Kovach, V.; Belousova, E.; Hegner, E.; Armstrong, R.; Dolgopolova, A.; Seltmann, R.; Alexeiev, D.V.; Hoffmann, J.E.; Wong, J.; et al. Reassessment of continental growth during the accretionary history of the Central Asian Orogenic Belt. *Gondwana Res.* **2014**, *25*, 103–125. [CrossRef]
20. Xiao, W.J.; Huang, B.; Han, C.; Sun, S.; Li, J. A review of the western part of the Altaids: A key to understanding the architecture of accretionary orogens. *Gondwana Res.* **2010**, *18*, 253–273. [CrossRef]
21. Xiao, W.; Windley, B.; Sun, S.; Li, J.; Huang, B.; Han, C.; Yuan, C.; Sun, M.; Chen, H. A tale of amalgamation of three collage systems in the Permian–Middle Triassic in Central-East Asia: Oroclines, sutures, and terminal accretion. *Annu. Rev. Earth Planet. Sci.* **2015**, *43*, 477–507. [CrossRef]
22. Li, P.; Sun, M.; Rosenbaum, G.; Jourdan, F.; Li, S.; Cai, K. Late Paleozoic closure of the Ob-Zaisan Ocean along the Irtysh shear zone (NW China): Implications for arc amalgamation and oroclinal bending in the Central Asian orogenic belt. *Geol. Soc. Am. Bull.* **2017**, *129*, B31541. [CrossRef]
23. Buslov, M.M. Tectonics and geodynamics of the Central Asian Foldbelt: The role of Late Paleozoic large-amplitude strike-slip faults. *Russ. Geol. Geophys. (Geol. I Geofiz.)* **2011**, *52*, 52–71. [CrossRef]
24. Buslov, M.M.; Cai, K. Tectonics and geodynamics of the Altai-Junggar orogen in the Vendian-Paleozoic: Implications for the continental evolution and growth of the Central Asian fold belt. *Geodyn. Tectonophys.* **2017**, *8*, 421–427. [CrossRef]
25. Buslov, M.M.; Shcerbanenko, T.A.; Kulikova, A.V.; Sennikov, N.V. Palaeotectonic reconstructions of the Central Asian folded belt in the Silurian Tuvaella and Retziella brachiopod fauna locations. *Lethaia* **2022**, *55*, 1–15. [CrossRef]
26. Ermolov, P.V.; Vladimirov, A.G.; Izokh, A.E.; Polyansky, N.V.; Revyakin, P.S.; Bortsov, V.D. *Orogenic Magmatism of Ophiolite Belts*; Nauka: Novosibirsk, Russia, 1983; p. 206. (In Russian)
27. Buslov, M.M.; Fujiwara, Y.; Safonova, I.Y.; Okada, S.; Semakov, N.N. The junction zone of the Gorny Altai and Rudny Altai terranes: Structure and evolution. *Geol. I Geofiz. (Russ. Geol. Geophys.)* **2000**, *41*, 383–397 (377–390).
28. Buslov, M.M.; Watanabe, T.; Fujiwara, Y.; Iwata, K.; Smirnova, L.V.; Safonova, I.Y.; Semakov, N.N.; Kiryanova, A.P. Late Paleozoic faults of the Altai region, Central Asia: Tectonic pattern and model of formation. *J. Asian Earth Sci.* **2004**, *23*, 655–671. [CrossRef]
29. Pirajno, F. Intracontinental strike-slip faults, associated magmatism, mineral systems and mantle dynamics: Examples from NW China and Altay-Sayan (Siberia). *J. Geodyn.* **2010**, *50*, 325–346. [CrossRef]
30. Dyachkov, B.A.; Bissatova, A.Y.; Mizernaya, M.A.; Zimanovskaya, N.A. Specific features of geotectonic development and ore potential in Southern Altai (Eastern Kazakhstan). *Geol. Ore Depos.* **2021**, *63*, 383–408. [CrossRef]
31. Travin, A.V.; Boven, A.; Plotnikov, A.V.; Vladimirov, V.G.; Tennisen, K.; Vladimirov, A.G.; Melnikov, A.I.; Titov, A.V. 40Ar/39Ar Dating of ductile deformations in the Irtysh Shear Zone, Eastern Kazakhstan. *Geochem. Int.* **2001**, *39*, 1237–1241.
32. Li, P.; Sun, M.; Rosenbaum, G.; Cai, K.; Chen, M.; He, Y. Transpressional deformation, strain partitioning and fold superimposition in the southern Chinese Altai, Central Asian Orogenic Belt. *J. Struct. Geol.* **2016**, *87*, 64–80. [CrossRef]
33. Xiao, W.; Han, C.; Yuan, C.; Sun, M.; Lin, S.; Chen, H.; Li, Z.; Li, J.; Sun, S. Middle Cambrian to Permian subduction-related accretionary orogenesis of North Xinjiang, NW China: Implications for the tectonic evolution of Central Asia. *J. Asian Earth Sci.* **2008**, *32*, 102–117. [CrossRef]
34. Li, P.; Sun, M.; Rosenbaum, G.; Cai, K.; Yu, Y. Structural evolution of the Irtysh Shear Zone (northwestern China) and implications for the amalgamation of arc systems in the Central Asian Orogenic Belt. *J. Struct. Geol.* **2015**, *80*, 142–156. [CrossRef]
35. Li, P.; Sun, M.; Rosenbaum, G.; Yuan, C.; Safonova, I.; Cai, K.; Jiang, Y.; Zhang, Y. Geometry, kinematics and tectonic models of the Kazakhstan Orocline, Central Asian Orogenic Belt. *J. Asian Earth Sci.* **2018**, *153*, 42–56. [CrossRef]
36. Li, P.; Sun, M.; Yuan Ch Jourdan, F.; Hu, W.; Jiang, Y. Late Paleozoic tectonic transition from subduction to collision in the Chinese Altai and Tianshan (Central Asia): New geochronological constraints. *Am. J. Sci.* **2021**, *321*, 178–205. [CrossRef]

37. Zhang, C.L.; Zou, H.B.; Yao, C.Y.; Dong, Y.G. Origin of permian gabbroic intrusions in the southern margin of the Altai Orogenic belt: A possible link to the permian tarim mantle plume? *Lithos* **2014**, *204*, 112–124. [CrossRef]
38. Khromykh, S.V.; Tsygankov, A.A.; Kotler, P.D.; Navozov, O.V.; Kruk, N.N.; Vladimirov, A.G.; Travin, A.V.; Yudin, D.S.; Burmakina, G.N.; Khubanov, V.B.; et al. Late paleozoic granitoid magmatism of Eastern Kazakhstan and Western Transbaikalia: Plume model test. *Russ. Geol. Geophys.* **2016**, *57*, 773–789. [CrossRef]
39. Navozov, O.V.; Solyanik, V.P.; Klepikov, N.A.; Karavaeva, G.S. Unsolved problems concerning the spatial and genetic relationship between some types of mineral resources and the intrusions of the Kalba–Narym and West Kalba zones of the Great Altai. *Geol. Conserv. Miner. Resour.* **2011**, *4*, 66–72. (In Russian)
40. Pirajno, F.; Ernst, R.E.; Borisenko, A.S.; Fedoseev, G.; Naumov, E.A. Intraplate magmatism in central Asia and China and associated metallogeny. *Ore Geol. Rev.* **2009**, *35*, 114–136. (In Russian) [CrossRef]
41. Chen, J.F.; Han, B.F.; Ji, J.Q.; Zhang, L.; Xu, Z.; He, G.Q.; Wang, T. Zircon U-Pb ages and tectonic implications of Paleozoic plutons in northern West Junggar, North Xinjiang, China. *Lithos* **2010**, *115*, 137–152. [CrossRef]
42. Polyakov, G.V.; Izokh, A.E.; Borisenko, A.S. Permian ultramafic-mafic magmatism and accompanying Cu-Ni mineralization in the Gobi-Tien Shan belt as a result of the Tarim plume activity. *Russ. Geol. Geophys.* **2008**, *49*, 455–467. [CrossRef]
43. Ernst, R.E. *Large Igneous Provinces*; Cambridge University Press: Cambridge, UK, 2014; 653p.
44. Li, Y.Q.; Li, Z.L.; Yu, X.; Langmuir, C.H.; Santosh, M.; Yang, S.F.; Chen, H.L.; Tang, Z.L.; Song, B.A.; Zou, S.Y. Origin of the Early Permian zircons in Keping basalts and magma evolution of the Tarim Large Igneous Province (northwestern China). *Lithos* **2014**, *204*, 47–58. [CrossRef]
45. Yarmolyuk, V.V.; Kuzmin, M.I.; Ernst, R.E. Intraplate geodynamics and magmatism in the evolution of the Central Asian Orogenic Belt. *J. Asian Earth Sci.* **2014**, *93*, 158–179. [CrossRef]
46. Dobretsov, N.L. Early Paleozoic tectonics and geodynamics of Central Asia: Role of mantle plumes. *Russ. Geol. Geophys. (Geol. I Geofiz.)* **2011**, *52*, 1539–1552. [CrossRef]
47. Khromykh, S.V.; Vladimirov, A.G.; Izokh, A.E.; Travin, A.V.; Prokop'ev, I.R.; Azimbaev, E.; Lobanov, S.S. Petrology and geochemistry of gabbro and picrites from the Altai collisional system of Hercynides: Evidence for the activity of the Tarim plume. *Russ. Geol. Geophys.* **2013**, *54*, 1288–1304. [CrossRef]
48. Ermolov, P.V.; Polyansky, N.V. Metamorphic complexes of the junction zone of the Rudny Altai and the rare-metal Kalba. *Geol. Geophys.* **1980**, *3*, 49–57. (In Russian)
49. Bespaev, K.A.; Polyansky, N.V.; Ganjenko, G.D.; Dyachkov, B.A.; Evtushenko, O.P.; Li, T.D. *Geology and Metallogeny of South-Western Altai (Within the Territory of Kazakhstan and China)*; Gylym: Almaty, Kazakhstan, 1997; 288p.
50. Khoreva, B.Y. *Geological Structure, Intrusive Magmatism and Metamorphism of the Irtysh Shear Zone*; Gosgeoltekhizdat: Moscow, Russia, 1963; 206p.
51. Chikov, B.M.; Zinoviev, S.V. Post-Hercynian (Early Mesozoic) collisional structures of Western Altai. *Russ. Geol. Geophys.* **1996**, *37*, 61.
52. Buslov, M.M.; Geng, H.; Travin, A.V.; Otgonbaatar, D.; Kulikova, A.V.; Chen, M.; Stijn, G.; Semakov, N.N.; Rubanova, E.S.; Abildaeva, M.A.; et al. Tectonics and geodynamics of Gorny Altai and adjacent structures of the Altai-Sayan folded area. *Russ. Geol. Geophys.* **2013**, *54*, 1250–1271. [CrossRef]
53. Briggs, S.M.; Yin, A.; Manning, C.E.; Chen, Z.L.; Wang, X.F.; Grove, M. Late Paleozoic tectonic history of the Ertix Fault in the Chinese Altai and its implications for the development of the Central Asian Orogenic System. *Geol. Soc. Am. Bull.* **2007**, *119*, 944–960. [CrossRef]
54. Zinov'ev, S.V.; Travin, A.V. The problem of dynamometamorphic transformations of rocks and ores of the upper part of the Ridder Sokol'noye deposit (Rudnyi Altai). *Dokl. Earth Sci.* **2012**, *444*, 738–742. [CrossRef]
55. Hodges, K.V. Geochronology and Thermochronology in Orogenic Systems. *Treatise Geochem.* **2004**, *3*, 263–292.
56. Ehlers, T.A. Crustal Thermal Processes and the Interpretation of Thermochronometer Data. *Rev. Mineral. Geochem.* **2005**, *58*, 315–350. [CrossRef]
57. Travin, A.V. Thermochronology of Early Paleozoic collisional and subductioncollisional structures of Central Asia. *Russ. Geol. Geophys.* **2016**, *57*, 434–450. [CrossRef]
58. Travin, A.V.; Buslov, M.M.; Bishaev, Y.A.; Tsygankov, A.A.; Mikheev, E.I. Late Paleozoic–Cenozoic Tectonothermal Evolution of Transbaikalia: Thermochronology of the Angara–Vitim Granitoid Batholith. *Russ. Geol. Geophys.* **2023**, *64*, 1086–1097. [CrossRef]
59. Dobretsov, N.L.; Borisenko, A.S.; Izokh, A.E.; Zhmodik, S.M. Thermochemical model of Permian mantle plumes of Eurasia as a basis for identifying patterns of formation and prediction of copper-nickel, noble and rare metal deposits. *Geol. Geophys.* **2010**, *51*, 1159–1187.
60. Kotler, P.D.; Khromykh, S.V.; Vladimirov, A.G.; Navozov, O.V.; Travin, A.V.; Karavaeva, G.S.; Murzintsev, N.G. New data on the age and geodynamic interpretation of the Kalba-Narym granitic batholith, eastern Kazakhstan. *Dokl. Earth Sci.* **2015**, *462*, 565–569. [CrossRef]

61. Khromykh, S.V.; Izokh, A.E.; Gurova, A.V.; Cherdantseva, M.V.; Savinsky, I.A.; Vishnevsky, A.V. Syncollisional gabbro in the Irtysh shear zone, Eastern Kazakhstan:nCompositions, geochronology, and geodynamic implications. *Lithos* **2019**, *346–347*, 105144. [CrossRef]
62. Xu, Y.G.; Wei, X.; Luo, Z.Y.; Liu, H.Q.; Cao, J. The early permian tarim large Igneous Province: Main characteristics and a plume incubation model. *Lithos* **2014**, *204*, 20–35. [CrossRef]
63. Lopatnikov, V.V.; Izokh, E.P.; Ermolov, P.V.; Ponomareva, A.P.; Stepanov, A.S. *Magmatism and Metallogeny of the Kalba-Narym Zone, Eastern Kazakhstan*; Nauka: Moscow, Russia, 1982; p. 248. (In Russian)
64. Dyachkov, B.A.; Mayorova, N.P.; Shcherba, G.N.; Abdrakhmanov, K.A. *Granitoid and Ore Formations of the Kalba-Narym Belt: Ore Altai*; Gylym: Almaty, Kazakhstan, 1994; 208p.
65. Savinskiy, I.A.; Vladimirov, V.G.; Sukhorukov, V.P. Chechek granite-gneiss structure (Irtysh shear zone). *Geol. I Pol. Iskop. Sib.* **2015**, *1*, 15–22. (In Russian with English abstract)
66. Savinskiy, I.A. Composition and isotopic characteristic of gneyss-granit of the Chechek Dome structure (Irtysh Shear Zone, East Kazakhstan). *Lithosphere* **2016**, *5*, 81–90. (In Russian)
67. Kotler, P.D.; Khromykh, S.V.; Kruk, N.N.; Sun, M.; Li, P.; Khubanov, V.B.; Semenova, D.V.; Vladimirov, A.G. Granitoids of the Kalba batholith, Eastern Kazakhstan: U–Pb zircon age, petroge nesis and tectonic implications. *Lithos* **2021**, *388–389*, 108056. [CrossRef]
68. Mar'in, A.M.; Nazarov, G.V.; Tkachenko, G.G.; Shulikov, E.S. *Geological Position and Age of Gabbro Intrusions in the Irtysh Fold Zone. Magmatism, Geochemistry and Metallogeny of Rudny Altai*; Nauka: Alma-Ata, Russia, 1966; pp. 32–45. (In Russian)
69. Kuzebny, V.S.; Vladimirov, A.G.; Ermolov, P.V.; Mar'in, A.M. Main types of gabbro intrusions in Zaisan folded system. In *Mafic-Ultramafic Complexes of Siberia*; Nauka: Novosibirsk, Russia, 1979; pp. 166–196. (In Russian)
70. Saetgaleeva, Y.; Kotler, P.D.; Kulikova, A.V. Thermal History of the Sibinsky Granitoid Massif (East Kazakhstan) According To Track Dating Data Apatite. In Proceedings of the XXX All-Russian Youth Conference Structure of the Lithosphere and Geodynamics, Irkutsk, Russia, 16–21 May 2023; Institute of the Earth's Crust SB RAS: Irkutsk, Russia, 2023.
71. Ludwig, K. *Isoplot 3.00: A Geochronological Toolkit for Microsoft Excel*; Berkeley Geochronology Center: Berkeley, CA, USA, 2003; p. 70.
72. Fleck, R.J.; Sutter, J.F.; Elliot, D.H. Interpretation of discordant 40Ar/39Ar age-spectra of Mesozoic tholeiites from Antarctica. *Geoch. Cosm. Acta* **1977**, *41*, 15–32. [CrossRef]
73. Wang, W.; Godard, V.; Liu-Zeng, J.; Zhang, J.; Li, Z.; Xu, S.; Yao, W.; Yuan, Z.; Aumaitre, G.; Bourlès, D.L.; et al. Tectonic controls on surface erosion rates in the Longmen Shan, Eastern Tibet. *Tectonics* **2021**, *40*, e2020TC006445. [CrossRef]
74. Wang, B.; Cluzel, D.; Jahn, B.-M.; Shu, L.; Chen, Y.; Zhai, Y.; Branquet, Y.; Barbanson, L.; Sizaret, S. Late paleozoic pre- and syn-kinematic plutons of the Kangguer–Huangshan Shear zone: Inference on the tectonic evolution of the eastern Chinese north Tianshan. *Am. J. Sci.* **2014**, *314*, 43–79. [CrossRef]
75. Tong, Y.; Wang, T.; Jahn, B.M.; Sun, M.; Hong, D.W.; Gao, J.F. Post-accretionary permian granitoids in the Chinese Altai orogen: Geochronology, petrogenesis and tectonic implications. *Am. J. Sci.* **2014**, *314*, 80–109. [CrossRef]
76. Tang, G.J.; Chung, S.L.; Hawkesworth, C.J.; Cawood, P.A.; Wang, Q.; Wyman, D.A.; Xu, Y.G.; Zhao, Z.H. Short episodes of crust generation during protracted accretionary processes: Evidence from Central Asian Orogenic Belt, NW China. *Earth Planet. Sci. Lett.* **2017**, *464*, 142–154. [CrossRef]
77. Hu, W.; Li, P.; Rosenbaum, G.; Liu, J.; Jourdan, F.; Jiang, Y.; Wu, D.; Zhang, J.; Yuan, C.; Sun, M. Structural evolution of the eastern segment of the Irtysh shear zone: Implications for the collision between the east Junggar Terrane and the Chinese Altai orogen (northwestern China). *J. Struct. Geol.* **2020**, *139*, 104126. [CrossRef]


**Disclaimer/Publisher's Note:** The statements, opinions and data contained in all publications are solely those of the individual author(s) and contributor(s) and not of MDPI and/or the editor(s). MDPI and/or the editor(s) disclaim responsibility for any injury to people or property resulting from any ideas, methods, instructions or products referred to in the content.